Petroleum Science 22 (2025) 4856–4874

Contents lists available at ScienceDirect

Petroleum Science

journal homepage: www.keaipublishing.com/en/journals/petroleum-science

Original Paper

Shale oil occurrence state and its controlling factors in saline lacustrine basins: Insights from sequential solvent extraction

Chen-Jia Zhang [a,b], Jian Cao [b,*], Bao-Li Xiang [c], Bao-Jian Shen [a], Ni Zhou [c], Wen-Yao Xiao [d,b], Yan Wang [b], Yu-Ce Wang [b], Xu-Sheng Guo [a]

[a] State Key Laboratory of Shale Oil and Gas Enrichment Mechanisms and Effective Development, Petroleum Exploration and Production Research Institute, SINOPEC, Beijing, 102206, China
[b] State Key Laboratory for Mineral Deposits Research, School of Earth Sciences and Engineering, Nanjing University, Nanjing, 210023, Jiangsu, China
[c] PetroChina Xinjiang Oilfield Company, Karamay, 834000, Xinjiang, China
[d] Key Laboratory of Petroleum Geochemistry, Research Institute of Petroleum Exploration and Development, China National Petroleum Corporation, Beijing, 100083, China

A R T I C L E I N F O

Article history:
Received 6 January 2025
Received in revised form
19 March 2025
Accepted 2 September 2025
Available online 6 September 2025

Edited by Jie Hao and Xi Zhang

Keywords:
Occurrence state
Sequential solvent extraction
Free hydrocarbons
Adsorbed hydrocarbons
Sweet spot

A B S T R A C T

Due to the complexity of the lithofacies associated with shale oil in saline lacustrine basins, the differences of shale oil occurrence state and its controlling factors in different lithofacies are not completely clear. This hinders efficient shale oil exploration and development. We investigated the shale oil in the Permian Lucaogou Formation in the Jimusar Sag, Junggar Basin, China, based mainly on sequential solvent extraction, petrological, organic geochemical, and nuclear magnetic resonance techniques. The fluidity of extractable organic matter decreased from the first extract to the fourth extract, which was caused by the gradual decrease in the contents of saturated and aromatic hydrocarbons, and gradual increase in the contents of NSO compounds and asphaltenes. The contents of free hydrocarbons (the first and second extracts) and adsorbed hydrocarbons (the third and fourth extracts) are very different among the lithofacies. The free hydrocarbon ratios in the siltstones and carbonate rocks are >70% and the main pore throats are >1 μm in size, corresponding to the best sweet spots. The contents of free hydrocarbons in the laminated silty mudstones and shales with bedding fractures are >50%, which are also available. The free hydrocarbons in the siltstones and carbonates are saturated with migrated hydrocarbons, with the contents being more affected by the physical properties of rocks. In contrast, the free hydrocarbons in the mudstones are mainly self-generated and -stored, and their contents are controlled by total organic carbon contents and maturity. For the adsorbed hydrocarbons, the contents in all lithofacies are controlled mainly by the total organic carbon contents. The biomarker parameters record a slight increase in maturity from the fourth to the first extract. The $\sum C_{22-}/\sum C_{23+}$ values of *n*-alkanes in the third extract are the lowest, because carbonate minerals tend to capture long-chain *n*-alkanes. The sequential solvent extraction method provides new insights into the occurrence state and molecular geochemical characteristics of lacustrine shale oil in different lithofacies. Future exploration should focus on siltstones and carbonate rocks with a relatively high proportion of the first extract (free hydrocarbons occurring in large pores and fractures), and mudstones with a relatively high proportion of the second extract (free to adsorbed hydrocarbons occurring in matrix pores) that are suitable for hydraulic fracturing to aid production.

1. Introduction

Shale oil is a major focus of global oil and gas exploration in the 21st century. China has undertaken considerable lacustrine shale oil exploration, and the amount of technically recoverable resources is 3×10^9 to 6×10^9 t, which is an important proportion of

* Corresponding author.
E-mail address: jcao@nju.edu.cn (J. Cao).
Peer review under the responsibility of China University of Petroleum (Beijing).

https://doi.org/10.1016/j.petsci.2025.09.003
1995-8226/

the global shale oil resources (Jarvie et al., 2007; Cardott, 2012; Uffmann et al., 2012; U. S. EIA, 2013; Tang et al., 2014; Zou et al., 2015, 2019). Unlike marine shale oil, lacustrine shale oil has a variety of occurrence states due to the complexity of properties of the crude oil and lithofacies (Jarvie, 2012; Zhang et al., 2018; Xiao et al., 2023; Falegnami et al., 2024a, 2024b). In addition, the different occurrence states restrict the shale oil fluidity. Therefore, for lacustrine shale oils, it is important to determine the shale oil contents and characteristics, and factors that control its enrichment in different occurrence states (Jarvie, 2012; Larter et al., 2012; Jiang et al., 2016; Li et al., 2016; Hu et al., 2021). Some studies have used multi-step Rock–Eval pyrolysis to characterize the occurrence states of shale oil (Sanei et al., 2015; Jiang et al., 2016; Romero-Sarmiento, 2019), and identify favorable production intervals (Jiang et al., 2016; Zhang et al., 2020; Hu et al., 2021; Wang et al., 2022a). Other studies have used 2D nuclear magnetic resonance (NMR) T_1–T_2 spectra to distinguish fluid components, such as light oil, heavy components, kerogen, and bound water in shale, which can reveal the degree of oil saturation and distribution of mobile fluids (Birdwell and Washburn, 2015; Song and Kausik, 2019; Li, 2020). Some previous studies have also analyzed the factors that affect shale oil fluidity by integrating qualitative (e.g., three-dimensional imaging) and quantitative (e.g., molecular dynamics simulations) methods, and have shown that high total organic carbon (TOC) contents increase the content of mobile hydrocarbons, as well as the adsorbed hydrocarbons (Lu et al., 2012; Hu et al., 2021; Zhao et al., 2021). An increase in thermal maturity leads to a decrease in the adsorption and expansion capacity of kerogen (Song et al., 2015; Wang et al., 2015, 2019), and the coupling of different minerals and organic carbon can also affect the adsorbed hydrocarbon contents (Raji et al., 2015; Li et al., 2016; Su et al., 2018; Ning et al., 2020). In general, shale oil is known to include free, adsorbed, swollen, and dissolved states, in which the available shale oil is dominated by the free and adsorbed states (Larter et al., 2012; Jiang et al., 2016; Li et al., 2016; Hu et al., 2021; Wang et al., 2022b). However, due to the complex chemical composition of shale oil and mineralogy of mixed fine-grained lacustrine source rocks, the occurrence state of shale oil in relation to different lithofacies remains unclear (Pan and Liu, 2009; Yang et al., 2015; Qian et al., 2017; Pan et al., 2018; Li et al., 2021; Zhang et al., 2023).

The Middle Permian Lucaogou Formation in the Jimusar Sag, Junggar Basin, is an important lacustrine shale oil exploration field in China. It is a typical saline lacustrine basin deposit and has been established as a national demonstration zone of shale oil (Kuang et al., 2012; Wang et al., 2023). The lithofacies in the basin are complex and heterogeneous (Tomassi et al., 2022, 2024), like most lacustrine shale oils (such as Yanchang Formation in Ordos Basin, Shahejie Formation in Jiyang Depression in Bohai Bay Basin, Funing Formation in Subei Basin, etc.), and the organic matter is low-mature to mature (Kuang et al., 2012; Cao et al., 2016; Wang et al., 2023; Zhang et al., 2023), and thus it is a typical example for the study of occurrence state of lacustrine shale oil. This is because, within complex lithofacies, the diversity of mineral components, pore types, and pore-throat structures complicates the occurrence states of shale oil. Therefore, for mixed siliciclastic-carbonate shale systems with such complexity, investigating the occurrence states of shale oil is even more critical. Meanwhile, in low-maturity to mature shale oil systems, organic matter has thermally decomposed to generate some liquid hydrocarbons but has not yet reached the stage of producing substantial gaseous hydrocarbons. At this stage, shale oil exists in distinct states, such as free and adsorbed states, which determine its mobility. Thus, in the exploration and development of such low-maturity to mature shale oil system, the occurrence state of shale oil directly dictate the recoverable value of the reservoir. Previous studies have carried out extensive research on the lithofacies, sedimentary depositional environment, hydrocarbon generation, and reservoir formation of the Lucaogou Formation (Kuang et al., 2012; Jiang et al., 2015; Qiu et al., 2016; Cao et al., 2016; Hu et al., 2018; Liu et al., 2019; Zhang et al., 2019b; Zhao et al., 2020; Wu et al., 2021; Olariu et al., 2022; Jiao et al., 2023; Jia et al., 2024). However, few studies have investigated the shale oil occurrence state and its controlling factors.

The sequential solvent extraction method can be used to determine the contents of hydrocarbons in different occurrence states, and also quantify the group composition and molecular geochemical characteristics of hydrocarbons in different occurrence state (including adsorbed oils that distinguish between different mineral surfaces and kerogen) (Pan and Liu, 2009; Pan et al., 2018; Li et al., 2021, 2023). Based on petrological observations, NMR and Rock–Eval pyrolysis data, we selected typical samples for the first application of the sequential solvent extraction technique to the Lucaogou Formation. We use these data to constrain the occurrence state of shale oil in different lithofacies in the fine-grained and heterogeneous strata of the formation. The molecular geochemical characteristics of the shale oil in different occurrence states were compared to determine how the shale oil formed. It is expected that our results can assist in the exploration for sweet spots and evaluations of shale oil resource potential in lacustrine basins, and are also relevant to hydrocarbon generation processes, primary hydrocarbon migration in source rocks, and shale oil exploration and production. This study will also have implications for the occurrence state and enrichment mechanism of shale oil in other saline lacustrine basins with similar mixed sedimentary lithofacies.

2. Geological setting

The Jimusar Sag is located in the southwestern region of the Eastern Uplift of the Junggar Basin (Fig. 1(a) and (b)), and covers an area of ~1500 km^2 (Kuang et al., 2012; Wang et al., 2023). In general, the sag has a relatively simple monocline-like structure with a gentle topography, and it has a continuous stratigraphy and only a few secondary faults. The western part of the sag is a low-lying area and the eastern part is a slope zone (Fig. 1(c)). The sag has experienced multiple cycles of tectonism and sedimentation (Allen and Natal'in, 1995; Fang et al., 2007; Zhang et al., 2021). It was formed in the late Carboniferous to Early Permian when the Jimusar fault was initially formed. The Bogeda Trough on the southern margin of the basin began to close orogenically in the late Early Permian, which caused the Jimusar Sag to begin to subsidence intensely, forming into a foreland dustpan-shaped sag. Until the middle to late Middle Permian, the study area further underwent strong subsidence with independent deposition, forming the main source rock of shale oil in this area (i.e., Lucaogou Formation). At the end of the late Triassic, influenced by the Indosinian orogeny, the sag began to uplift greatly, and part of the Permian and Triassic strata in the eastern slope were denuded. During the Cretaceous period, due to the influence of Yanshanian orogeny, the tectonic activities of the Jimusar Sag were slightly active. The southeast part of the sag gradually uplifted and contracted to the northwest, and the independent pattern disappeared. Until the Paleogene and Quaternary periods, under the influence of Himalayan orogeny, the Bogeda Mountains to the south of the sag were uplifted rapidly and thrust towards the center of the basin. The strata in the Jimusar Sag gradually thinned from west to east, and the present tectonic pattern is formed.

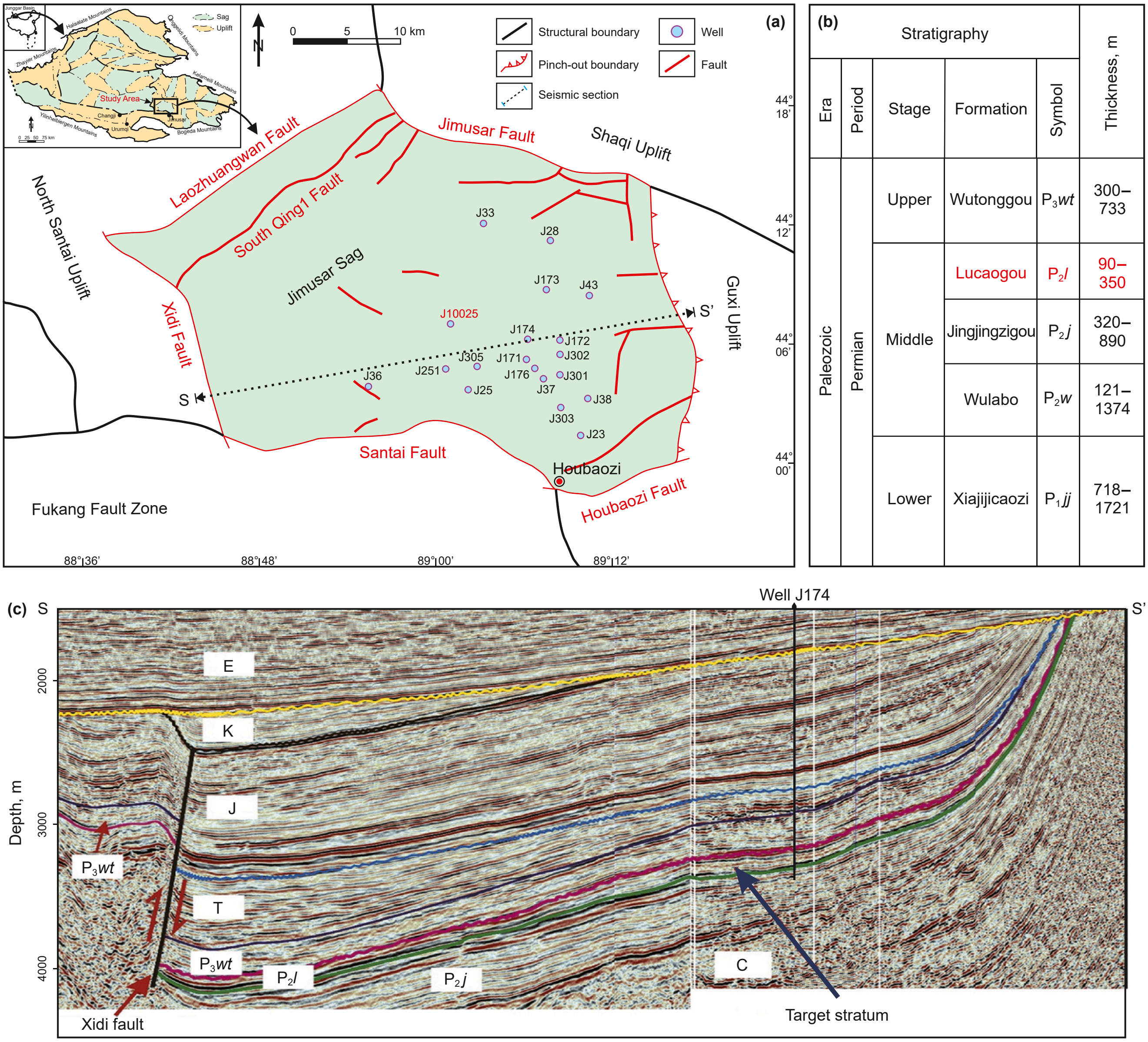

Fig. 1. Structural and stratigraphic framework of the Jimusar Sag. (**a**) Location, structural features, and well locations. (**b**) Permian strata and thicknesses. (**c**) N–S seismic profile.

The Lucaogou Formation was deposited mainly in a deep saline lake, with some strata also deposited in shallow to semi-deep lake and delta facies. The burial depth of the formation is 2500–4500 m, and the Lucaogou Formation has a thickness of 90–350 m (Xiao et al., 2008; Kuang et al., 2012; Zhi et al., 2019). The lithofacies in the Lucaogou Formation are complex and variable, including abundant terrigenous and carbonate rocks, and a small amount of pyroclastic rocks. The rock types include carbonate rocks, dolomitic/calcareous mudstone, silty mudstone, tuffaceous mudstone, and siltstone. Tuff is distributed sporadically and, in general, there are four main rock types: carbonate rocks, dolomitic/calcareous mudstone, silty mudstone, and siltstone (Zhang et al., 2023; Zhi et al., 2023). Based on oil production results and logging data, the two intervals with the best oil output are termed the upper sweet spot (mainly $P_2l_2^2$) and lower sweet spot (mainly $P_2l_1^2$), a thick mudstone occurs between the two sweet spots (Kuang et al., 2012; Jiang et al., 2015). The crude oil produced from the upper and lower sweet spots is mainly heavy oil, with a density of 0.88–0.92 g/cm^3 (Wang et al., 2023).

3. Samples and methods

This study focuses on well J10025, including samples of the Lucaogou Formation from different intervals, which have variable lithofacies and oil contents. Nine samples were analyzed, including one siltstone, two carbonate rocks, three silty mudstones (shales), and three dolomitic mudstones. The aim was to apply the sequential solvent extraction technique, group component separation, and gas chromatography (GC) and GC-mass spectrometry (MS) analysis, underpinned by basic petrological observations, TOC and Rock–Eval pyrolysis analyses, and NMR T_2 experiments.

3.1. Petrology

Samples were cut perpendicular to bedding and made into thin-sections (Amijaya and Littke, 2006). An optical microscope was used to observe the thin-sections. The light source for the transmitted and reflected light observations was a 100 W halogen lamp, and fluorescence was examined using a 100 W Hg lamp, which was excited by blue light.

3.2. Organic geochemistry

The TOC contents were measured with an organic chemical element analyzer. Before the analyses, the samples were powdered to 100 mesh, treated with 10% HCl for 36 h to remove inorganic carbonate, centrifuged with deionized water to remove the acid, and finally dried at 60 °C.

Rock–Eval pyrolysis was undertaken with a Rock–Eval VI pyrolysis instrument. Samples were powdered to <100 mesh and placed in a He atmosphere and heated at 300 °C for 3 min to obtain the free hydrocarbon content (S_1 in mg HC/g rock). The temperature was then increased to 600 °C at a rate of 25 °C/min to obtain the hydrocarbon content generated by kerogen pyrolysis (S_2 in mg HC/g rock). The temperature corresponding to the S_2 peak was the pyrolysis peak temperature (T_{max}).

3.3. NMR T_2 spectra experiments

The NMR T_2 spectra were obtained with a nanopore analyzer. The experimental parameters were as follows: waiting time = 5000 ms; echo number = 2048; echo interval = 0.1 ms; and number of scans = 128. The software for the instrument (NMR Analysis application software) has converted the spin echo string attenuation data into the distribution of transverse relaxation time (T_2), which in turn is converted to the pore size. The longer the transverse relaxation time, the larger the pore size (transverse relaxation time >10 ms, corresponds to pore size >1 μm). To mitigate the influence of retained oil, this study employed parallel sample protocols: the original sample was split into two portions. One sub-sample designated for NMR testing underwent prior Soxhlet extraction for 72 h to remove retained oil. Prior to the analyses, the samples were cut into cylindrical shapes with diameters of 1.5 cm and heights of 1 cm. All the samples were analyzed twice, the first time on the original samples and the second time after the samples had been saturated with deionized water for 12 h under vacuum. The first analyses (i.e., the background values) were subtracted from the second analyses, which yielded the actual pore size distribution curve of the samples. This method is to characterize the pore scale of different lithofacies. And combined with hydrocarbon contents in different occurrence states, the reservoir capacity and the corresponding fluidity of shale oil in various lithofacies can be analyzed.

3.4. Sequential solvent extraction

The sequential solvent extraction method was optimized based on Pan et al. (2018). The detailed experimental steps were as follows. Firstly, 50 g of sample was dried at 50 °C and crushed to a 5–10 mm particle size, and then a mixed solvent of 93:7 dichloromethane and methanol was used for extraction for 72 h. The extractable organic matter (EOM) obtained in this step is EOM-A. After freezing and drying the extracted sample residue, the sample was gently powdered to 150 mesh and extracted with chloroform in a Soxhlet extractor for 72 h to obtain EOM-B. The extracted sample residue was frozen and dried, weighed and placed in a beaker, slowly mixed with 50% HCl (1:1; v/v), and heated in a water bath at 70 °C for 3 h while stirring to ensure the carbonate minerals were fully dissolved. After cooling, the solution/residue was transferred to a plastic centrifuge bottle, centrifuged to remove the aqueous solution, mixed with ultra-pure water, and rinsed repeatedly until the solution was pH neutral. After lyophilizing the sample residue, it was freeze-dried and extracted with the Soxhlet extractor for 72 h. The soluble organic matter obtained in this step is EOM-C. The residual rock sample was weighed again and placed in a polyethylene plastic bottle, treated repeatedly with a mixture of HF and 50% HCl (1:2; v/v), and heated in a water bath at 70 °C for 3 h to dissolve the silicate minerals. The sample residue after acid hydrolysis was freeze-dried and extracted with chloroform in a Soxhlet extractor for 72 h. The soluble organic matter obtained in this step is EOM-D.

EOM-A is soluble organic matter occurring in large pores and fractures in a free state. EOM-B is mainly soluble organic matter occurring in matrix pores with poorer mobility compared to EOM-A (free hydrocarbons in large fractures/pores), thus EOM-B may represent a transitional state between free and adsorbed hydrocarbons, termed the “free to adsorbed state”. EOM-C is organic matter that is tightly bound to, or included within carbonate minerals. And EOM-D is organic matter that is tightly bound to, or included within clay minerals or kerogens by chemisorption. Therefore, the retained soluble organic matter can be defined as being in the free state (EOM-A), free to adsorbed state (EOM-B), and adsorbed state (EOM-C and -D) according to the different occurrence states. The novelty and uniqueness of our method may be that it not only changed the crushing degree of samples (EOM-A is from the bulk sample; EOM-B is from the powder sample), but also selected different pretreatment and extraction solvents according to previous studies.

3.5. Group component separation and GC/GC-MS analysis

The rock extracts obtained in each step from the sequential solvent extraction were separated into group components. Firstly, an appropriate amount of *n*-hexane was added and asphaltene was precipitated. After repeated filtration, the asphaltene was collected with methylene chloride, and the filtrate was used for the separation of other group components by column chromatography. The chromatographic columns were filled with an appropriate amount of pre-extracted absorbent cotton, and 3 g of activated silica gel and 1 g of alumina were evenly added to the column and compacted. The samples were transferred to the chromatographic columns and then eluted with *n*-hexane, a *n*-hexane and dichloromethane mixture (Hex: CH_2Cl_2 = 7:3, v/v), and a dichloromethane and methanol mixture (CH_2Cl_2: CH_3OH = 1:1, v/v). The saturated hydrocarbon, aromatic hydrocarbon, and non-hydrocarbon (colloidal) components were then separated.

GC and GC-MS were used to analyze the saturated hydrocarbon components in the extracts of each step from the sequential solvent extraction, using a Neptune Plus multi-collector mass spectrometer (Thermo-Fisher; Germany). The GC analysis was performed with a HP-6890 gas chromatograph. The chromatographic column was a HP-5 elastic quartz capillary column (30 m × 0.32 mm), with a fixed phase film thickness of 0.25 μm and N_2 carrier gas. During the analysis, the initial temperature of the GC oven was 80 °C (5 min) and it was then increased to 290 °C at 4 °C/min. The GC-MS analysis was undertaken with HP6890 and Agilent 5973N chromatographs using He as the carrier gas. The initial temperature of the GC oven was 60 °C (5 min), and then the temperature was increased to 120 °C at 8 °C/min and to 290 °C at 2 °C/min. The temperature was then held constant for 30 min.

4. Results

4.1. Petrological features

The Lucaogou Formation in the Jimusar Sag contains mainly a mixture of terrigenous clastic and fine-grained authigenic carbonate sedimentary rocks, which are primarily dolomite and mudstone. The classification of the multisource mixed rocks is detailed in Zhang et al. (2021), in which the three-level nomenclature (10%, 25%, and 50%) was followed, and the rock structures were also taken into account when further classifying the rock types (e.g., laminae). For the textures and fabrics of carbonate rocks, the presence or absence of carbonate mud, which differentiates muddy carbonate from grainstone. In this study, nine samples were analyzed, including one dolomitic siltstone (Fig. 2(a)) and two carbonate rock samples, which were a dolarenite (Fig. 2(b)) and silty marl (Fig. 2(c)) that both contain a large amount of organic matter (Fig. 2(b) and (c)). Three samples of silty mudstone (shale) were also analyzed, with sample J-174 being a mudstone with silty laminae (Fig. 2(d)) and samples J-1 and J-146 being shales with obvious laminae that contain a large amount of organic matter (Fig. 2(e) and (f)). Three samples of dolomitic mudstone were also analyzed, which contain idiomorphic dolomite, fine silt, and abundant organic matter (Fig. 2(g)–(i)).

4.2. Micro-fluorescence features

In general, the microscopic occurrence of residual hydrocarbons (shale oil) in rocks can be divided into the following main types (Xie et al., 2016; Kus et al., 2017; Pickel et al., 2017). (1) Hydrocarbons occur in irregular microfractures or large intergranular pores and appear yellow or brown in fluorescence; (2) Hydrocarbons occur in the mineral matrix, showing yellow fluorescence in the visual field, and the structure is difficult to distinguish; (3) Hydrocarbons are adsorbed on the surface of the mineral and fluoresce more brightly than mineral particles that do not adsorb hydrocarbons; (4) Hydrocarbons are bound to kerogen and emit bright fluorescence, which are not easy to distinguish. The nine samples have different micro-fluorescence characteristics (Fig. 3). In general, the siltstones and carbonate rocks have better physical properties and more abundant storage space, and the hydrocarbons exhibit yellow–green to green fluorescence, are mainly in the free state, and occur mostly in dissolution and intergranular pores (Fig. 3(a)–(c)). In the laminated shale, the hydrocarbons occur in bedding fractures in the free state, and the fluorescence is typical of oily asphalt distributed along bedding fractures or adsorbed on mineral surfaces, which is difficult to observe, but exhibits dark yellow to yellowish brown fluorescence (Fig. 3(d)–(f)). The degree of pore development in the mudstone with a less-laminated structure is relatively poor, and hydrocarbons occur mostly in the matrix, which is difficult to observe (Fig. 3(g)–(i)).

4.3. Organic geochemistry

The Rock–Eval pyrolysis and TOC data show that samples with different lithologies have a variable hydrocarbon generation potential. TOC contents of the nine samples are >2.0 wt%, except for samples J-180, J-174, and J-140; PG values ($S_1 + S_2$) of the

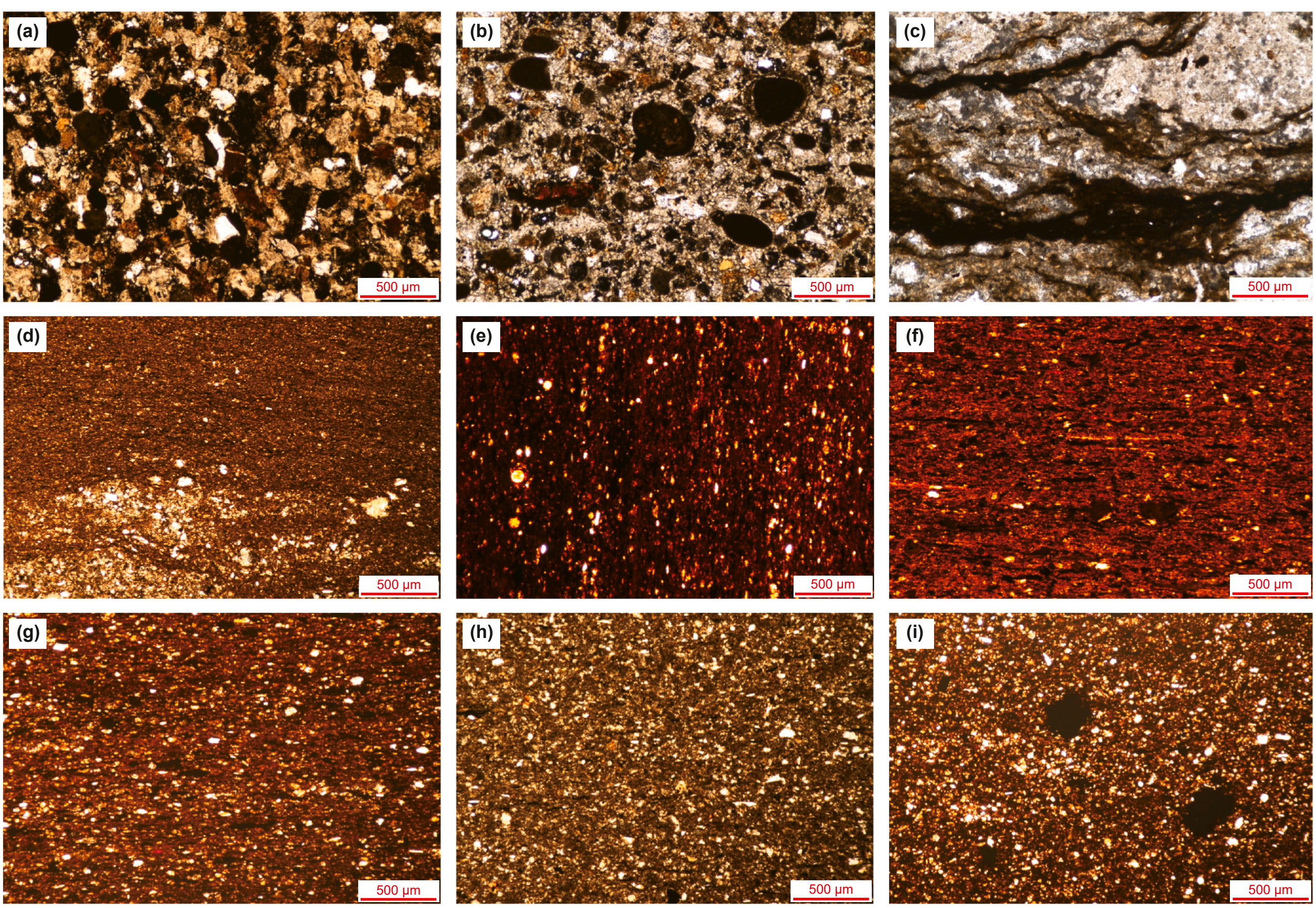

Fig. 2. Photomicrographs of the nine samples and main lithologies in the Lucaogou Formation, Jimusar Sag. (**a**) Sample J-140 from 3559.31 m depth (dolomitic siltstone); (**b**) sample J-138 from 3552.58 m depth (dolarenite); (**c**) sample J-127 from 3531.33 m depth (silty marl); (**d**) sample J-174 from 3693.96 m depth (silty mudstone); (**e**) sample J-1 from 3510.41 m depth (silty shale); (**f**) sample J-146 from 3575 m depth (silty shale); (**g**) sample J-176 from 3698.12 m depth (dolomitic mudstone); (**h**) sample J-180 from 3709.19 m depth (dolomitic mudstone); and (**i**) sample J-184 from 3729.33 m depth (dolomitic mudstone).

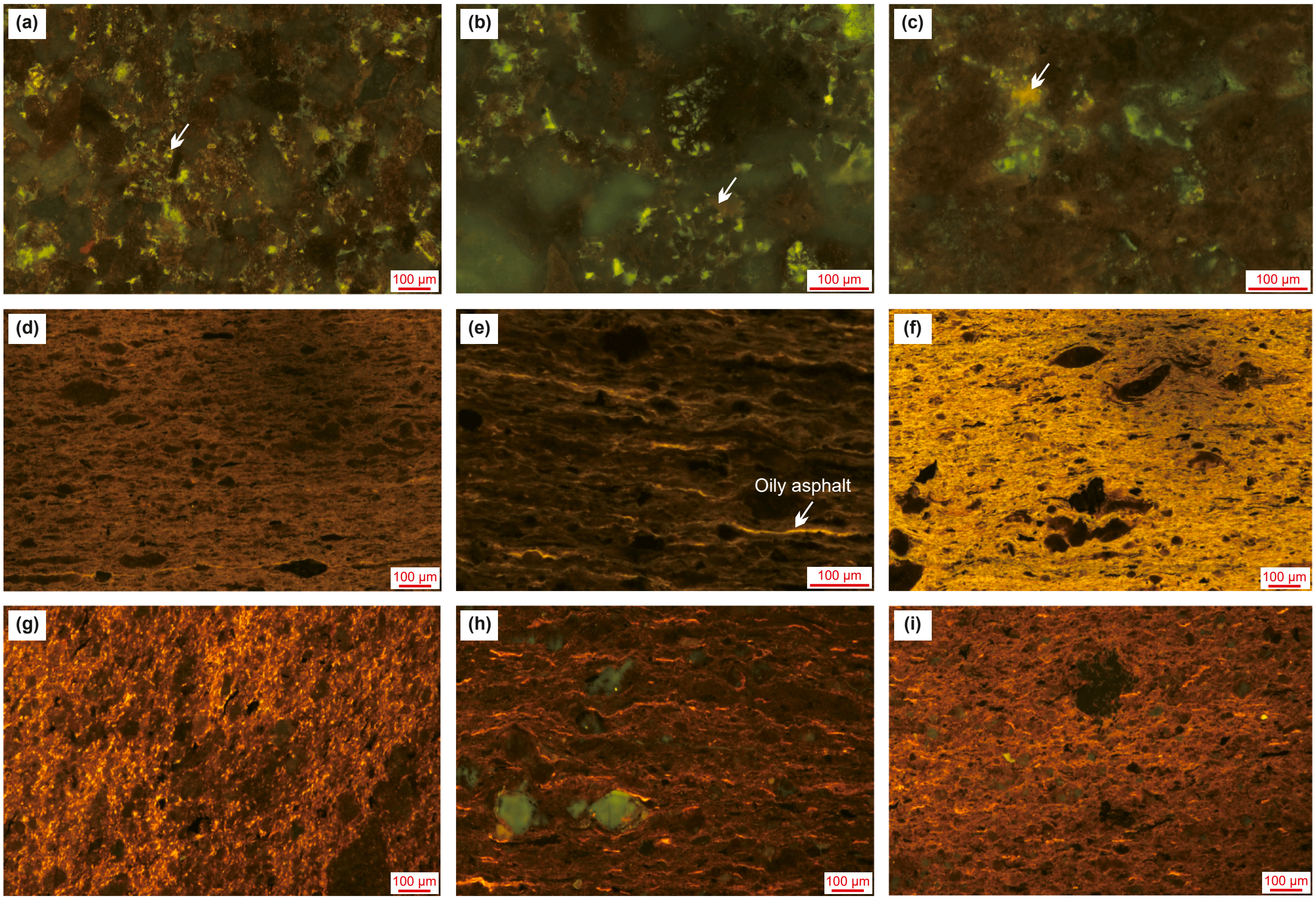

Fig. 3. Fluorescence photographs of the nine samples and main lithologies in the Lucaogou Formation, Jimusar Sag. (**a**) Sample J-140 from 3559.31 m depth (dolomitic siltstone); (**b**) sample J-138 from 3552.58 m depth (dolarenite); (**c**) sample J-127 from 3531.33 m depth (silty marl); (**d**) sample J-174 from 3693.96 m depth (silty mudstone); (**e**) sample J-1 from 3510.41 m depth (silty shale); (**f**) sample J-146 from 3575 m depth (silty shale); (**g**) sample J-176 from 3698.12 m depth (dolomitic mudstone); (**h**) sample J-180 from 3709.19 m depth (dolomitic mudstone); and (**i**) sample J-184 from 3729.33 m depth (dolomitic mudstone). White arrows indicate hydrocarbons that can be observed.

remaining samples are >20 mg/g (Table 1), indicating the hydrocarbon generation potential is good, particularly for the mudstones. The organic matter is mostly types I and II_1, and the T_{max} values indicate the samples are low-mature and close to or have reached the oil generation peak. The silty shale (sample J-146) has the best hydrocarbon generation potential. The carbonate rock and siltstone have the highest OSI values ($S_1 \times 100$/TOC, mg HC/g TOC) and best shale oil potential.

4.4. Reservoir space

The NMR T_2 spectra of the pore size distribution at the nanometer–micrometer-scale show that the siltstone and carbonate rocks mostly have a wide, low-amplitude, unimodal to weakly bimodal distribution, with the main peak having a large pore size (mostly micrometer-scale; Fig. 4(a)–(c)). However, the main pore size peaks of the silty mudstone and dolomitic mudstone are narrow with a high amplitude, and are nanometer-scale (Fig. 4(d)–(i)). The pore size distribution range of the main peaks is 0.001–0.1 μm (Fig. 4(d) and (g)–(i)). If there are complex components present in a sample (e.g., mineral laminae), the pore size distribution exhibits greater heterogeneity and can be bimodal (Fig. 4(d)). The two shale samples have a high-amplitude, unimodal pore size distribution, with the pore size mainly being on a nanometer-scale but the maximum distribution range is more than 0.1 μm (Fig. 4(e) and (f)), which is slightly larger than for the

Table 1
TOC and Rock–Eval pyrolysis data for nine samples of different lithologies from the Lucaogou Formation in the Jimusar Sag.

Lithology	Sample No.	Depth, m	TOC, %	T_{max}, °C	S_1, mg/g	S_2, mg/g	S_3, mg/g	HI, mg/g	PG, mg/g	OSI, mg/g
Dolomitic siltstone	J-140	3559.31	4.51	426	11.22	7.17	0.65	158.94	18.39	248.72
Dolarenite	J-138	3552.58	7.21	426	19.52	13.17	1.11	182.56	32.69	270.58
Silty marl	J-127	3531.33	14.70	432	10.57	10.58	0.80	71.97	21.15	71.90
Silty mudstone	J-174	3693.96	3.61	436	1.63	16.93	0.30	469.10	18.56	45.16
Silty shale	J-1	3510.41	9.73	447	4.45	47.76	0.37	490.75	52.21	45.72
Silty shale	J-146	3575.00	27.08	456	1.92	158.28	0.70	499.53	137.20	7.08
Dolomitic mudstone	J-176	3698.12	13.09	440	2.65	91.10	1.04	695.79	93.75	20.23
Dolomitic mudstone	J-180	3709.19	2.01	437	0.78	6.92	0.88	343.59	7.70	38.72
Dolomitic mudstone	J-184	3729.33	6.68	450	1.14	39.67	0.54	593.50	40.81	17.05

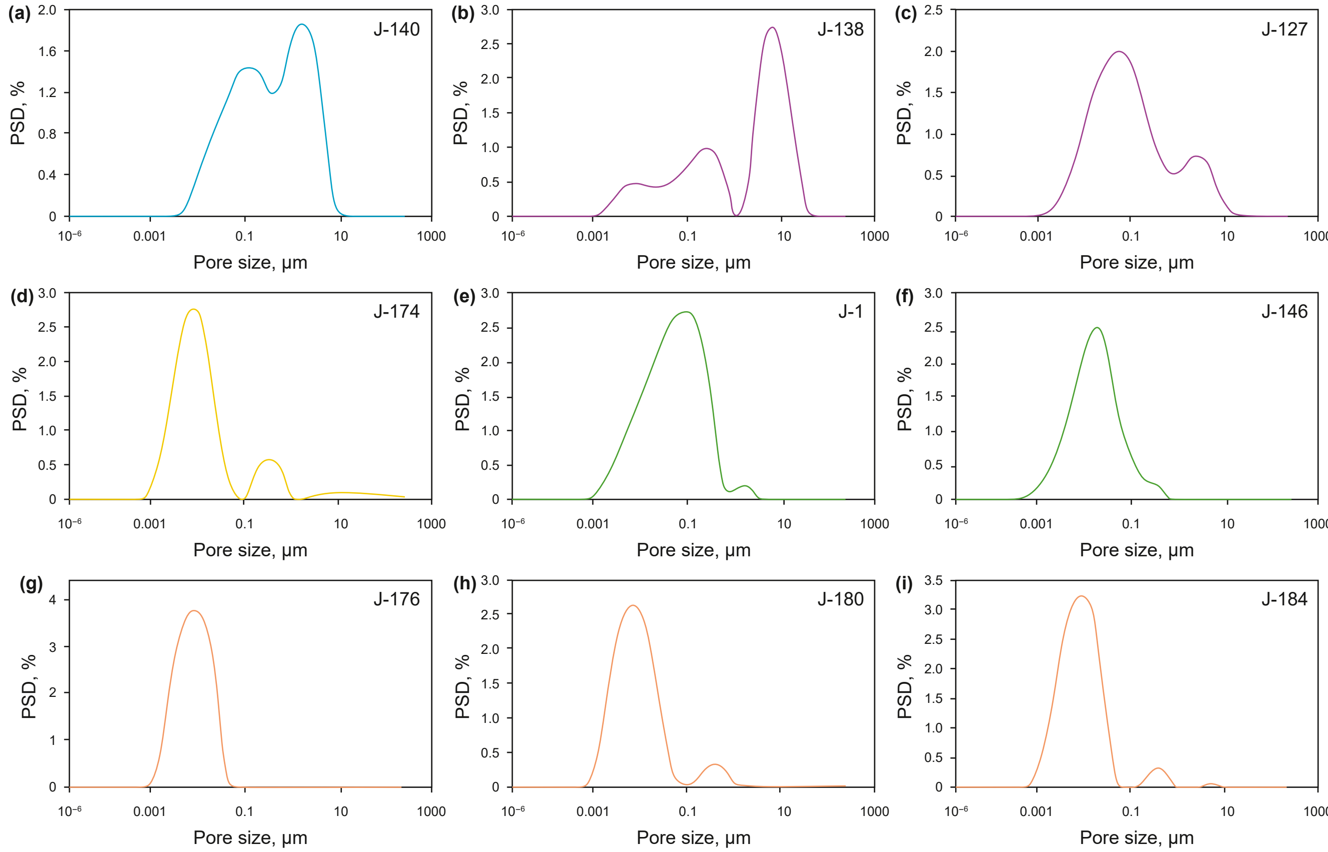

Fig. 4. NMR T_2 spectra of nine samples of different lithologies from the Lucaogou Formation, Jimusar Sag. (**a**) Sample J-140 from 3559.31 m depth (dolomitic siltstone); (**b**) sample J-138 from 3552.58 m depth (dolarenite); (**c**) sample J-127 from 3531.33 m depth (silty marl); (**d**) sample J-174 from 3693.96 m depth (silty mudstone); (**e**) sample J-1 from 3510.41 m depth (silty shale); (**f**) sample J-146 from 3575 m depth (silty shale); (**g**) sample J-176 from 3698.12 m depth (dolomitic mudstone); (**h**) sample J-180 from 3709.19 m depth (dolomitic mudstone); and (**i**) sample J-184 from 3729.33 m depth (dolomitic mudstone). The logarithmic scales are used for the X-axes.

mudstone. The development of bedding fractures improves the physical properties of the reservoirs. In summary, the carbonate rocks and siltstones contain mostly micrometer-sized pores, with a wide distribution of pore size and good physical properties. The pore size distributions of the mudstones are heterogeneous and these rocks contain nanometer-scale pores.

4.5. Sequential solvent extraction

The sequential solvent extraction results are shown in Table 2 and Fig. 5. The EOM-A contents in siltstone sample J-140 and carbonate samples J-138 and J-127 are the highest, being 46.20, 45.08, and 37.16 mg/g, respectively. The EOM-C and -D contents are low. In contrast, the mudstones have the opposite features. Their EOM-A contents are low and EOM-C and -D contents are high (Table 2; Fig. 5). For example, the EOM-C contents in the silty shale sample J-146 and dolomitic mudstone sample J-180 are 1.91 and 1.52 mg/g, and the EOM-D contents are 4.78 and 3.92 mg/g, respectively. Although the TOC content of the silty shale is the highest of the nine samples (27.08 wt%), its EOM-A content is much lower than those of the siltstones and carbonate rocks. In addition, the EOM-A contents of the shale samples J-146 and J-1 (13.36 and 3.68 mg/g; Table 2) are higher than those of the other mudstones, indicative of higher free oil contents in large pores.

5. Discussion

5.1. Differences in shale oil occurrence state among the analyzed lithologies

The shale oil in the different lithologies can be generally divided into two types: the free and adsorbed states (the swollen

Table 2
Sequential solvent extraction data for nine samples of different lithologies from the Lucaogou Formation in the Jimusar Sag.

Lithology	Sample No.	Depth, m	TOC, %	EOM-A, mg/g	EOM-B, mg/g	EOM-C, mg/g	EOM-D, mg/g
Dolomitic siltstone	J-140	3559.31	4.51	46.32	0.55	0.68	0.24
Dolarenite	J-138	3552.58	7.21	45.08	4.31	0.88	4.09
Silty marl	J-127	3531.33	14.70	37.16	2.60	0.65	7.55
Silty mudstone	J-174	3693.96	3.61	2.69	0.95	0.64	0.28
Silty shale	J-1	3510.41	9.73	3.68	0.71	0.46	0.75
Silty shale	J-146	3575.00	27.08	13.36	4.69	1.91	4.78
Dolomitic mudstone	J-176	3698.12	13.09	4.44	3.15	1.52	3.92
Dolomitic mudstone	J-180	3709.19	2.01	2.46	1.97	1.09	1.47
Dolomitic mudstone	J-184	3729.33	6.68	3.84	2.84	1.23	2.82

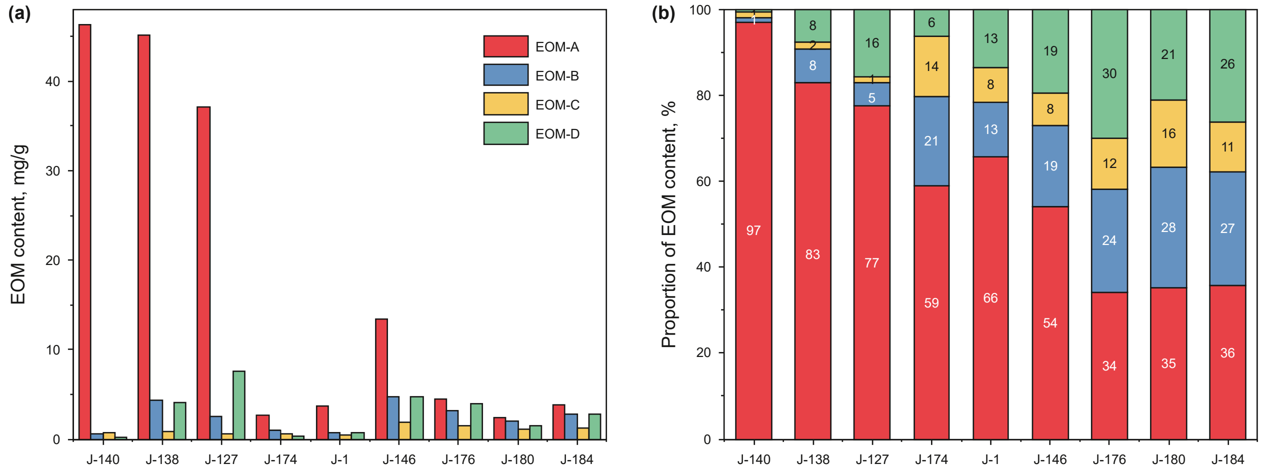

Fig. 5. Hydrocarbon contents in different lithologies from the Lucaogou Formation in the Jimusar Sag (J-140: Dolomitic siltstone; J-138: Dolarenite; J-127: Silty marl; J-174: Silty mudstone; J-1: Silty shale; J-146: Silty shale; J-176: Dolomitic mudstone; J-180: Dolomitic mudstone; J-184: Dolomitic mudstone). (**a**) Absolute contents of the four extracts from the nine samples. (**b**) Relative contents of the four extracts from the nine samples.

and dissolved states were not readily identifiable by petrological observations). The hydrocarbons mostly exhibited bright yellow to yellowish brown micro-fluorescence (Fig. 3), indicating the oils are heavy with little difference in maturity (Khorasani, 1987; Zhang et al., 2019a).

The results of the sequential solvent extraction from the different lithofacies are significantly different (Fig. 5). The absolute EOM-A content in the siltstone is the highest (Table 3; Fig. 5(a)), accounting for 96.91% of the total extract (Figs. 5(b) and 6(a)). The average proportion of EOM-A in the carbonate rocks is 80.2% (Fig. 6(b)), which highlights that these two lithofacies are high-quality reservoir rocks in the Lucaogou Formation, and contain high free oil contents in large pores and fractures.

The proportion of free oil in the silty mudstone and silty shale is also relatively high (Fig. 6(c) and (d)), which may be related to the development of the silty laminae and bedding fractures. The EOM-A and -B contents of the silty shale are significantly higher than those of all the other mudstones (Table 2; Fig. 5(a)), which may be related to the development of bedding fractures that improve the reservoir physical properties (Fig. 2(e) and (f)) and a higher free hydrocarbon content. For the dolomitic mudstones, the proportions of EOM-A and -B are the lowest of all the lithologies (Fig. 6(e)), and the absolute contents are also low (Table 2; Fig. 5(a)), indicating that adsorbed oil dominates in this lithofacies (Fig. 6(e)). It is worth noting that the proportion of EOM-B in this lithology is up to 26.3%, which is the highest of all the lithologies (Fig. 6(e)). Considering that some isolated pores in rocks are opened to solvents by crushing, the extraction rate is increased, similar to hydraulic fracturing during shale oil production (Tamimi and Uysal, 1990; Wei et al., 2014). Therefore, EOM-B can represent the oil production capacity after hydraulic fracturing, and thus the dolomitic mudstone can have a greatly improved shale oil output after fracturing.

In summary, the free hydrocarbon contents of the siltstones, carbonate rocks, and silty shales are high, and especially the siltstones and carbonate rocks occur in the high-quality target sweet spots. The silty and dolomitic mudstones have high adsorbed hydrocarbon contents, but can also form sweet spots. Hydraulic fracturing could greatly increase the free oil productivity of the dolomitic mudstones.

5.2. Controls on the shale oil occurrence state

The occurrence state of shale oil is controlled by numerous factors, especially the abundance of organic matter, hydrocarbon generation capacity, and reservoir properties. In this study, the

Table 3
Chromatographic parameters of the saturated hydrocarbons in the four extracts from the four lithologies in the Lucaogou Formation, Jimusar Sag.

Lithology	Sample No.	Hydrocarbon of different occurrence states	Main peak of carbon	Peak pattern	$\Sigma C_{22-}/\Sigma C_{23+}$	Pr/Ph	CPI	OEP
Dolomitic siltstone	J-140 (J10025, 3559.31 m)	EOM-A	C_{21}	unimodal	1.74	1.06	1.21	1.16
		EOM-B	C_{23}	unimodal	1.07	1.09	1.29	1.16
		EOM-C	C_{21}	unimodal	1.50	2.36	1.26	1.06
		EOM-D	C_{23}	unimodal	1.50	0.91	1.24	1.13
Dolarenite	J-138 (J10025, 3552.58 m)	EOM-A	C_{23}	unimodal	0.92	1.06	1.29	1.17
		EOM-B	C_{23}	unimodal	0.79	1.22	1.10	1.20
		EOM-C	C_{21}	unimodal	1.33	2.34	1.25	1.11
		EOM-D	C_{23}	unimodal	1.73	1.02	1.32	1.16
Silty shale	J-146 (J10025, 3575 m)	EOM-A	C_{21}	unimodal	3.59	1.72	0.83	1.14
		EOM-B	C_{21}	unimodal	1.16	1.45	1.03	1.16
		EOM-C	C_{25}	unimodal	0.99	0.64	1.35	1.18
		EOM-D	C_{21}	unimodal	1.72	0.63	1.48	1.20
Dolomitic mudstone	J-180 (J10025, 3709.19 m)	EOM-A	C_{23}	bimodal	1.34	1.32	1.07	1.14
		EOM-B	C_{31}	bimodal	1.03	1.18	1.10	1.15
		EOM-C	C_{17}	bimodal	0.70	1.05	1.13	1.17
		EOM-D	C_{17}	bimodal	1.41	1.02	1.29	1.20

Note: $\text{CPI} = 1/2 \times \left[\sum(C_{25}\text{–}C_{33})/\sum(C_{24}\text{–}C_{32}) + \sum(C_{25}\text{–}C_{33})/\sum(C_{26}\text{–}C_{34})\right]$, $\text{OEP} = (C_{21} + 6C_{23} + C_{25})/(4 \times C_{22} + 4 \times C_{24})$

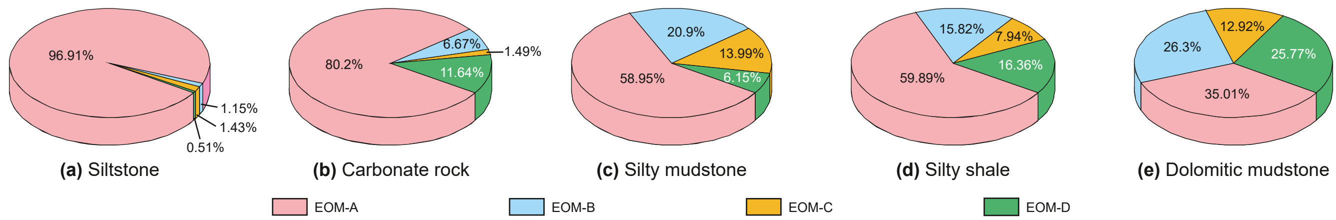

Fig. 6. Average proportions of soluble organic matter with different occurrence states in different lithologies. The average proportions of EOM with different occurrence states are shown for (**a**) siltstone, (**b**) carbonate rocks, (**c**) silty mudstone, (**d**) silty shale, and (**e**) dolomitic mudstone.

absolute content of free soluble organic matter (the sum of EOM-A and -B) of the siltstones and carbonate rocks is high, but has no obvious relationship with TOC contents (Fig. 7(a)), indicating there may be migrated free oil in these reservoir rocks, and the content of free oil in reservoir rocks is not controlled by TOC. The absolute content of adsorbed oil (the sum of EOM-C and D) was positively correlated with TOC value. In addition, the content of adsorbed oil in the silty shales and dolomitic mudstones is significantly positively correlated with TOC content (Fig. 7(a)), indicating the adsorbed oil content in all lithofacies is controlled by the TOC content. It is worth noting that the free hydrocarbon content of the silty shales and dolomitic mudstones is also significantly positively correlated with TOC content (Fig. 7(a)). Because the pores in the mudstones are mainly mesopores smaller than 10 nm (Fig. 4(d)–(i)), the capillary resistance inside the mesopores restricts the fluid flow (Wang et al., 2015; Zhang et al., 2014; Huang et al., 2020), resulting in a large amount of residual oil in the mudstones. For the self-generating and -storing mudstone reservoirs, when the thermal evolution degree is in a certain stage, both the free and adsorbed oil contents are controlled by the TOC contents. In contrast, the siltstones and carbonate rocks have lower TOC contents and better physical properties (Fig. 4(a)–(c)), and the free oil content is mainly affected by migrated hydrocarbons and controlled by the physical properties of the reservoir.

By comparing the relative proportions of free and adsorbed hydrocarbons in the different lithofacies, it is evident that TOC content is negatively correlated with the proportion of free oil and positively correlated with the proportion of adsorbed oil

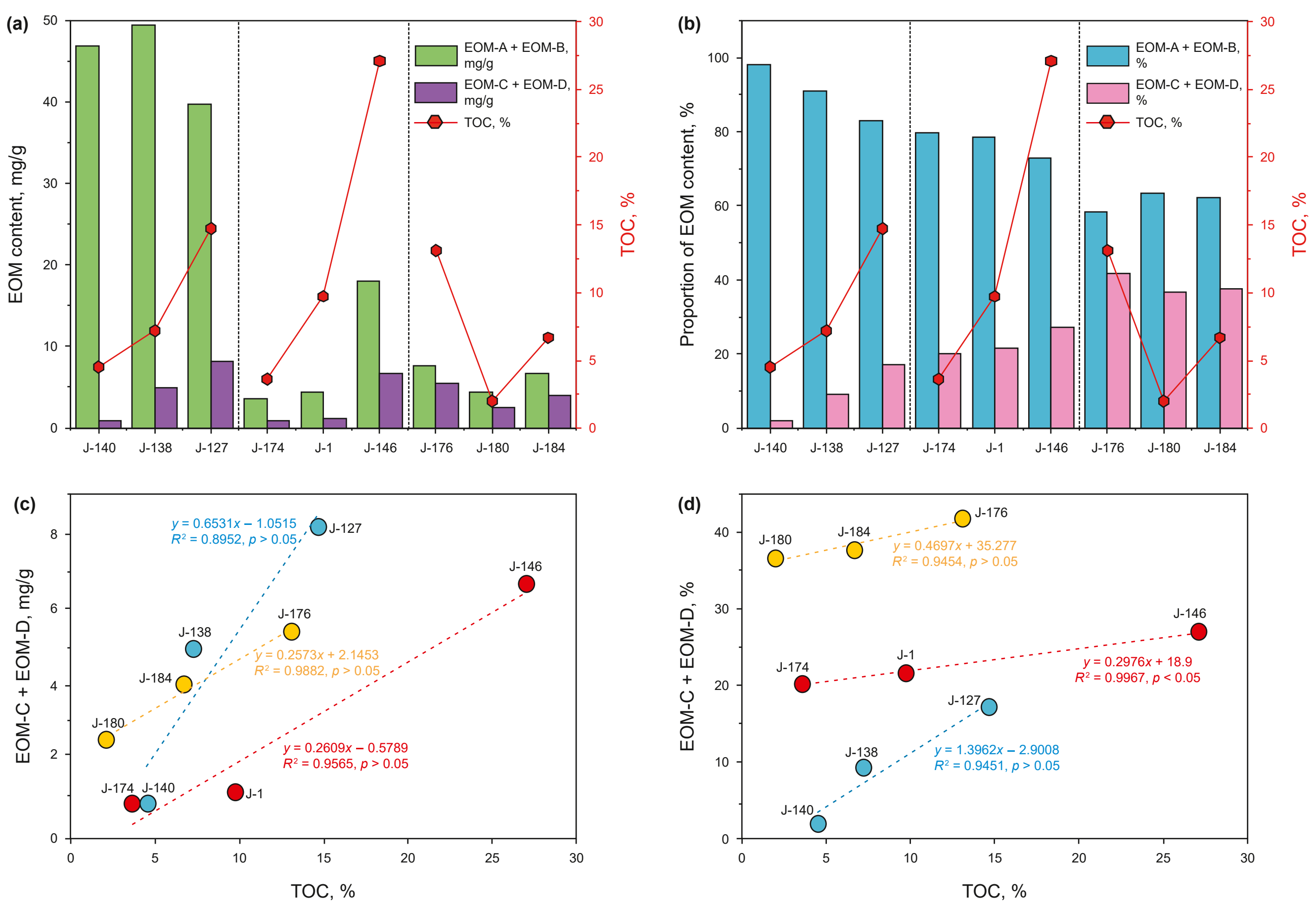

Fig. 7. Average proportions of soluble organic matter in the different lithofacies (J-140: Dolomitic siltstone; J-138: Dolarenite; J-127: Silty marl; J-174: Silty mudstone; J-1: Silty shale; J-146: Silty shale; J-176: Dolomitic mudstone; J-180: Dolomitic mudstone; J-184: Dolomitic mudstone). (**a**) Free and adsorbed hydrocarbon contents as compared with TOC contents. (**b**) Relative proportions of free and adsorbed hydrocarbon contents as compared with TOC contents. (**c**) Correlation analyses of TOC and adsorbed oil contents. (**d**) Correlation analyses of TOC contents and relative proportions of adsorbed hydrocarbon contents.

(Fig. 7(b)). This further indicates that the adsorbed oil contents are mainly controlled by the TOC contents. In summary, the lithology and physical properties control the free oil contents in low-mature shale oil systems, such as the Lucaogou Formation. More specifically, The free oil contents of reservoir rocks such as carbonate rocks and siltstones are more affected by physical properties, and the free oil contents of mudstones are controlled by TOC contents. The adsorbed oil contents of all lithologies are mainly controlled by TOC contents.

The free hydrocarbon contents in lacustrine shale reservoirs are not only affected by the lithology (i.e., physical properties), but also the thermal maturity (Lu et al., 2012; Jiang et al., 2016, 2020; Pan et al., 2018; Hu et al., 2021). A comparative analysis of the sequential solvent extraction results for the three silty mudstone (shale) samples and three dolomitic mudstone samples in the low-mature to mature stage with different T_{max} values shows that, for a given lithology, the proportion of EOM-A increases with increasing T_{max} (i.e., thermal maturity; Fig. 8). This may be related to the compositional characteristics of low-mature crude oil in the early stages of oil generation, such as low contents of saturated hydrocarbons, low saturation/aromatic ratios, and high contents of non-hydrocarbons (Spiro, 1984; Pan et al., 2018). When the maturity is low, the crude oil viscosity is higher and its migration ability is weak. However, with increasing thermal evolution, many mobile small molecules are formed, which enhances the hydrocarbon migration ability, and thus the proportion of mobile free hydrocarbons also increases.

The group compositional characteristics of free hydrocarbons extracted from the three silty shales and three dolomitic mudstones (i.e., EOM-A and -B) were further analyzed (Fig. 9). For samples with higher T_{max} values (i.e., maturity), the saturated hydrocarbon percentage of EOM-A and -B is higher, indicating that more small-molecular hydrocarbon compounds are formed during thermal evolution, which increases the hydrocarbon migration ability and proportion of mobile free hydrocarbons (Dickey, 1975; Pan et al., 2018). As such, the relative contents of free hydrocarbons are affected by the thermal maturity.

An interesting phenomenon is that the relative contents of saturated hydrocarbons in the four extracts from the nine samples (Fig. 10) show that the siltstones and carbonate rocks have a relatively high proportion of free hydrocarbons (EOM-A and -B) (Figs. 5(b) and 6(a)–(b), and 7(b)) and also the highest proportion of saturated hydrocarbons in free oil. This demonstrates that the shale oil in these rocks has the highest fluidity, followed by that in the shales and then the silty mudstones. This further shows that the free oil content is controlled by the rock physical properties and that the hydrocarbon occurrence space and pore connectivity of the different lithologies are variable, which affect the porosity and permeability. During migration, oil and gas always preferentially occupy large pores in the free state or by physical adsorption. After these favorable spaces are occupied, organic matter will gradually enter mesopores and micropores (or matrix pores) (Yang et al., 2015; Li et al., 2022). Therefore, with little change in maturity, the lithology controls the reservoir physical properties, which in turn affect the distribution of mobile free hydrocarbons in lacustrine shale oil systems.

5.3. *Significance of molecular biomarkers in shale oil with different occurrence states*

Fig. 11 shows the molecular compositional characteristics of the saturated hydrocarbons in the four extracts from four lithologies. The four lithologies have some common characteristics, such as the saturated hydrocarbons in EOM-A and -B (Fig. 11(a)–(b), (e)–(f), (h)–(j), and (m)–(n)), and thus the occurrence state of EOM-A and -B are indeed similar, mainly the free states. The adsorbed hydrocarbons (i.e., EOM-C and -D) in each lithology are significantly different in terms of the biomarker characteristics of EOM-A and -B (Fig. 11(c)–(d), (g)–(h), (k)–(l), and (o)–(p)), particularly for the dolomitic siltstone (Fig. 11(c) and (d)) and dolarenite (Fig. 11(g) and (h)). This further indicates that the physical properties of these two lithologies are better than those of the mudstones (Fig. 4), and they are reservoirs in the Lucaogou Formation that accommodate near-source hydrocarbon migration and accumulation of EOM-A and -B (Qiu et al., 2016; Zhang et al., 2023). Therefore, studies of the variations of molecular characteristics of hydrocarbons with different occurrence states in the same lithologies should focus on the mudstones. In general, the distribution of saturated hydrocarbons in the four extracts from the two types of mudstone samples (J-146 and J-180) are similar, respectively. However, sample J-180 has an unresolved complex mixture (UCM) peak (Fig. 11(m)–(p)), which may be due to biodegradation to a certain extent (Peters, 1986).

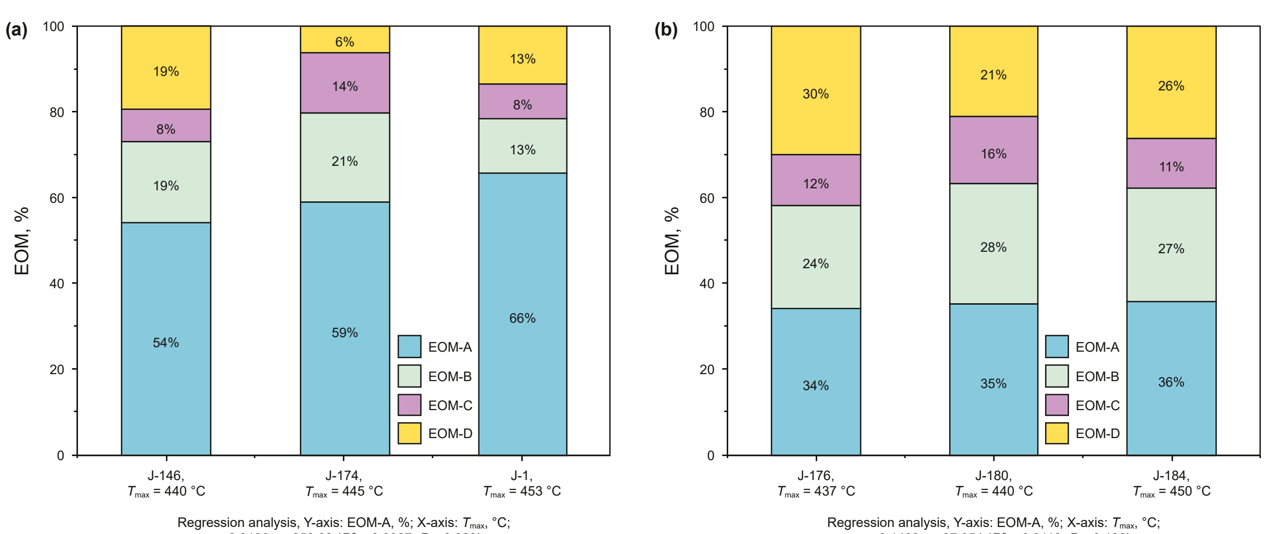

Fig. 8. Proportion of hydrocarbons in different occurrence states in mudstones of different maturities. The proportion of hydrocarbons (i.e., the four EOM types) is shown in the (**a**) three silty shale samples with different maturities and (**b**) three dolomitic mudstone samples with different maturities.

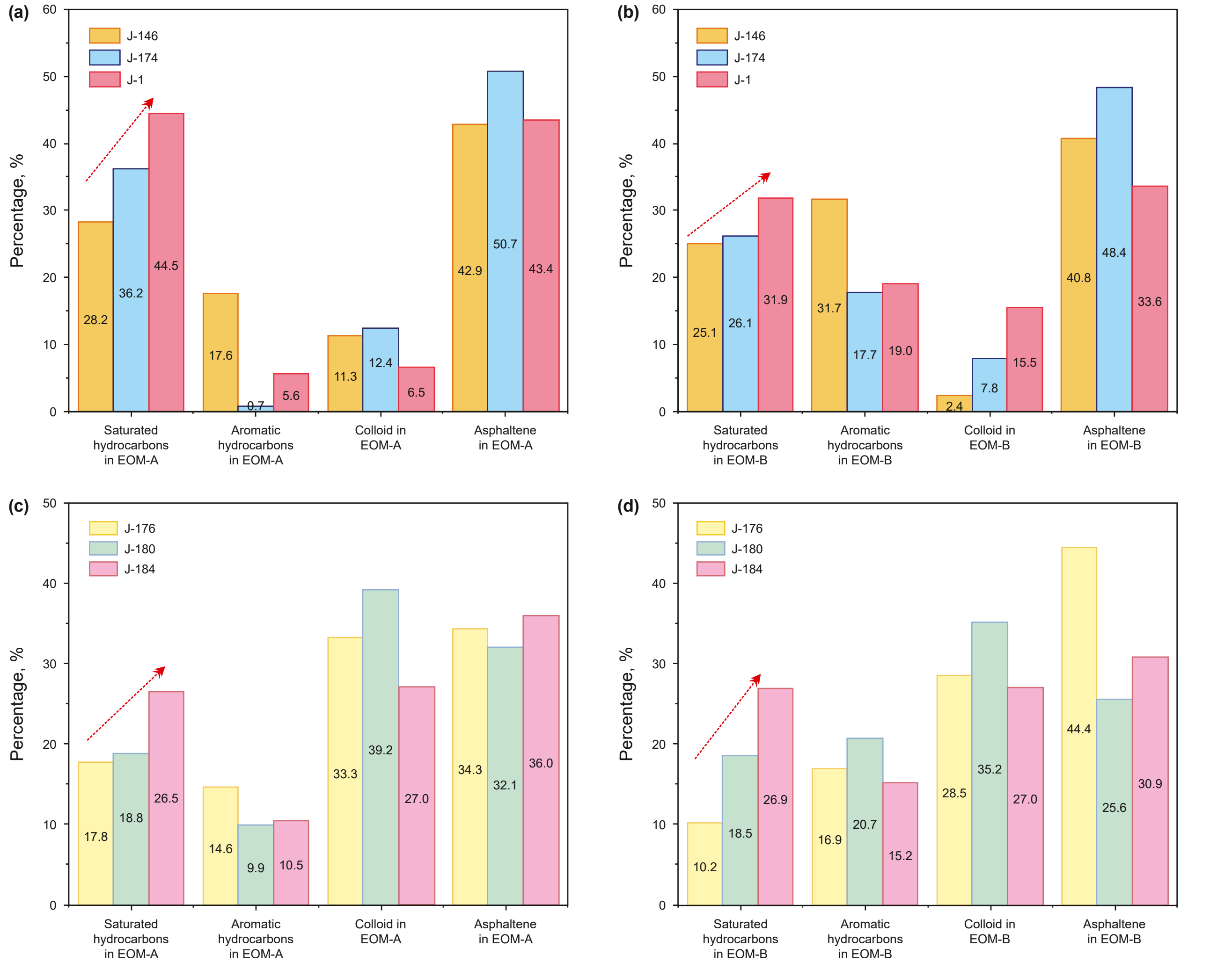

Fig. 9. Comparison of the group compositions of mudstones with different maturities. Group composition of (**a**) EOM-A in three samples of silty mudstone (shale), (**b**) EOM-B in three samples of silty mudstone (shale), (**c**) EOM-A in three samples of dolomitic mudstone, and (**d**) EOM-B in three samples of dolomitic mudstone.

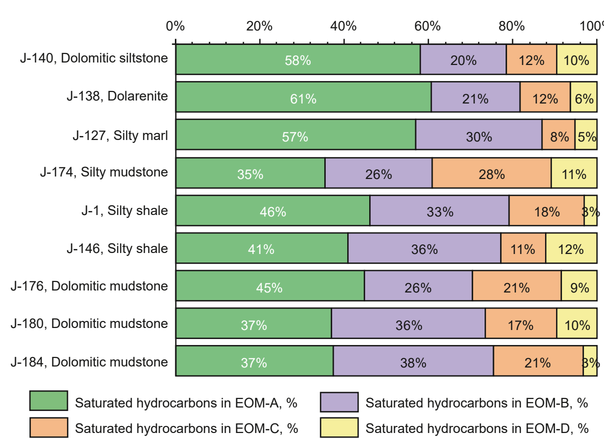

Fig. 10. Proportions of saturated hydrocarbons in different occurrence states in samples of different lithologies.

5.3.1. N-alkanes and isoprenoids

Taking the silty shale sample J-146 as an example (Fig. 11(i)–(l)), the molecular characteristics of hydrocarbons in different occurrence states were analyzed. In general, an odd–even predominance (OEP) of the *n*-alkanes is not obvious, which is typical of mature source rocks. From EOM-A to -D, the carbon numbers increase slightly and the carbon number range of EOM-A is C_{12}–C_{33}, whereas that of EOM-D is C_{14}–C_{33}, indicating that the heavy components of adsorbed hydrocarbons were slightly dominant. The main carbon peak of the saturated hydrocarbons in EOM-A, -B, and -D is C_{21}, and the main peak in EOM-C is C_{23}, with the latter having the lowest $\sum C_{22-}/\sum C_{23+}$ value (0.99; Fig. 12(c); Table 3). The dolomitic mudstone sample J-180 also has a low $\sum C_{22-}/\sum C_{23+}$ value, with that for EOM-C being the lowest (0.7; Fig. 12(d)), indicating that carbonate minerals in the source rocks tend to contain early formed, long-chain *n*-alkanes (Yang et al., 2015). The $\sum C_{22-}/\sum C_{23+}$ values of saturated hydrocarbons in EOM-A and -D from the two mudstone samples are higher than those of saturated hydrocarbons in EOM-B and -C (Fig. 12(c) and (d); Table 3). This is because EOM-A is mainly free soluble organic matter, while the saturated hydrocarbon components are mainly weakly polar or non-polar compounds. They occur in EOM-A in a free state or weak physical adsorption state. EOM-D is the soluble organic matter closely bound to silicate minerals or kerogen, and the soluble organic matter adsorbed between clay minerals, especially smectite layers, is mainly saturated hydrocarbons with relatively low carbon numbers (Guan et al., 1998). In addition, EOM-D has a high

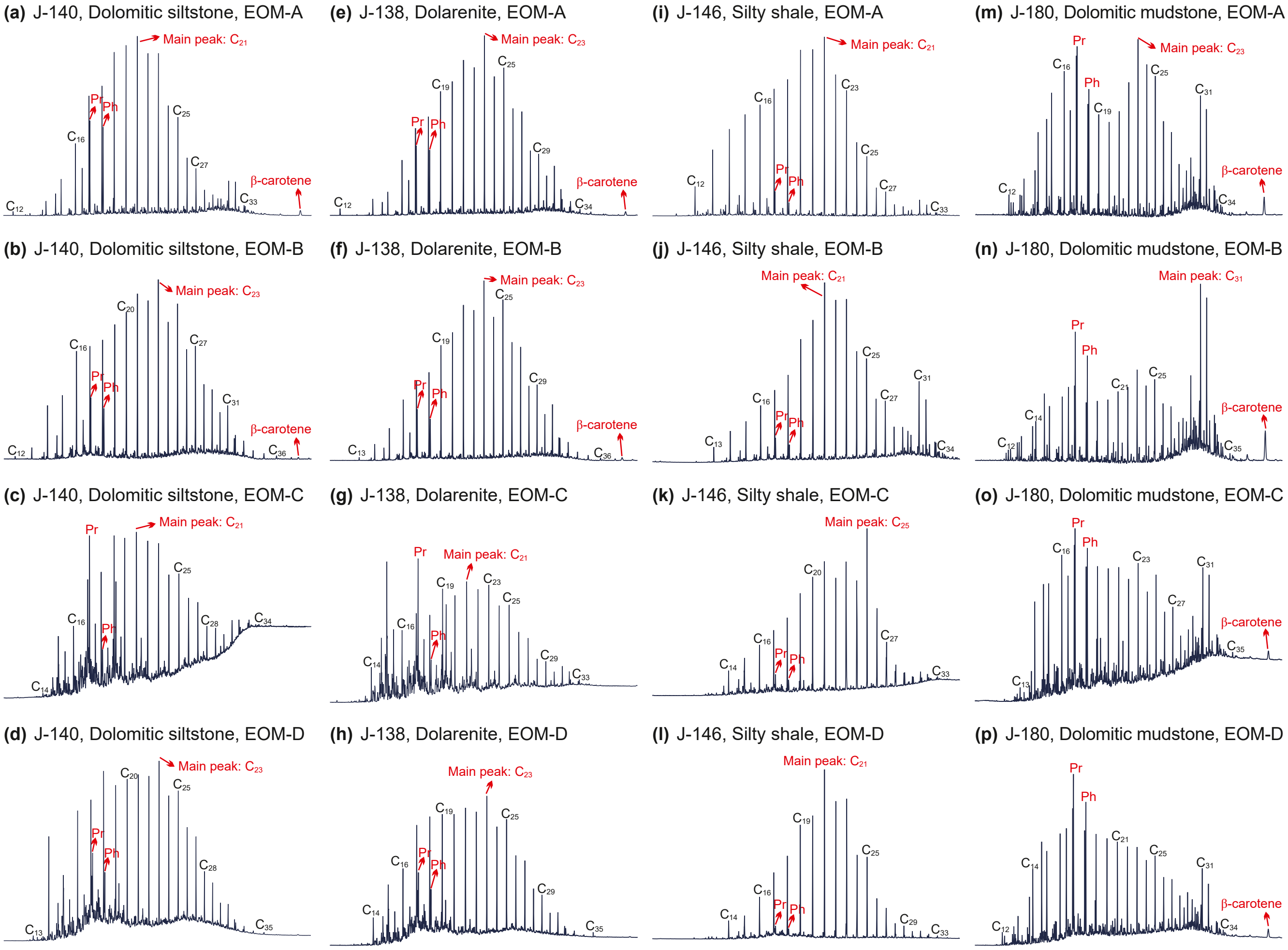

Fig. 11. Gas chromatograms of saturated hydrocarbons in the four extracts from the four lithologies of the Lucaogou Formation, Jimusar Sag.

content of gum and asphaltene, which can adsorb some weakly polar or non-polar molecules (Yang et al., 2015; Pan et al., 2018). Therefore, EOM-D contains a high proportion of low-carbon number, saturated hydrocarbons.

Based on the changes in the normal alkane parameters of the four extracts from the mudstone samples J-146 and J-180 (Table 3; Fig. 12(c) and (d)), the carbon preference index (CPI) and OEP values of EOM-D to -A decrease gradually, indicating that EOM-A has the highest maturity and EOM-D the lowest maturity. This is because hydrocarbons included in minerals have a lagged evolution, which hinders the degree of cracking of long-chain into short-chain hydrocarbons. As a result, they have a lower maturity and usually preserve the geochemical characteristics of earlier formed oil and gas in the source rock (Spiro, 1984; Guan et al., 1998; Pan et al., 2018), whereas EOM-A and -B are continuously discharged during hydrocarbon generation and have relatively higher maturity. In addition, the Pr/Ph ratio varies in the four extracts from the two types of mudstone, with a slight decrease in the Pr/Ph ratio from EOM-A to -D (Table 3; Fig. 12(c) and (d)). Given the sedimentary depositional environment of a given rock must be largely constant, the change in the Pr/Ph ratio of the shale oil with different occurrence states is likely controlled by the maturity, because the Pr/Ph ratio of organic matter increases with increasing maturity (Mei and Liu, 1980; Koopmans et al., 1999). As such, the Pr/Ph ratios further show the increase in maturity from EOM-D to -A, which is consistent with the CPI and OEP proxies.

The maturity parameters of siltstone sample J-140 and carbonate sample J-138 do not exhibit above trends, showing that the maturity of EOM-D is slightly less than that of EOM-C, but there is no gradual trend between between it and EOM-A and -B (Table 3; Fig. 12(a) and (b)), which further indicates that the free hydrocarbons in the siltstones and carbonate rocks are mainly migrated hydrocarbons. The mudstones are dominated by retained hydrocarbons.

5.3.2. Steranes and terpanes

The characteristics of the terpanes and steranes indicate that the $m/z = 191$ and $m/z = 217$ spectra of the four lithologies are not significantly different, and only the peak heights are slightly different. Taking samples J-146 and J-180 of the two types of mudstone as examples (Table 4; Fig. 13), the contents of tricyclic terpanes increase slightly from EOM-A to -D, and the ratios of tricyclic terpanes to pentacyclic triterpanes of sample J-146 are 0.14, 0.16, 0.10, and 0.04, respectively. The ratios of tricyclic terpanes to pentacyclic triterpanes for sample J-180 are 0.15, 0.15, 0.16, and 0.10, respectively (Table 4). Although the ratios of tricyclic terpanes to pentacyclic triterpanes are not very different, the maturity of EOM-D to -A increases slightly. The T_s/T_m values also exhibit similar characteristics, which are generally consistent with the maturity features recorded by the ratios of tricyclic terpanes to pentacyclic triterpanes, and CPI and OEP values. However, the T_s/T_m values of the four extracts from the dolomitic mudstone sample

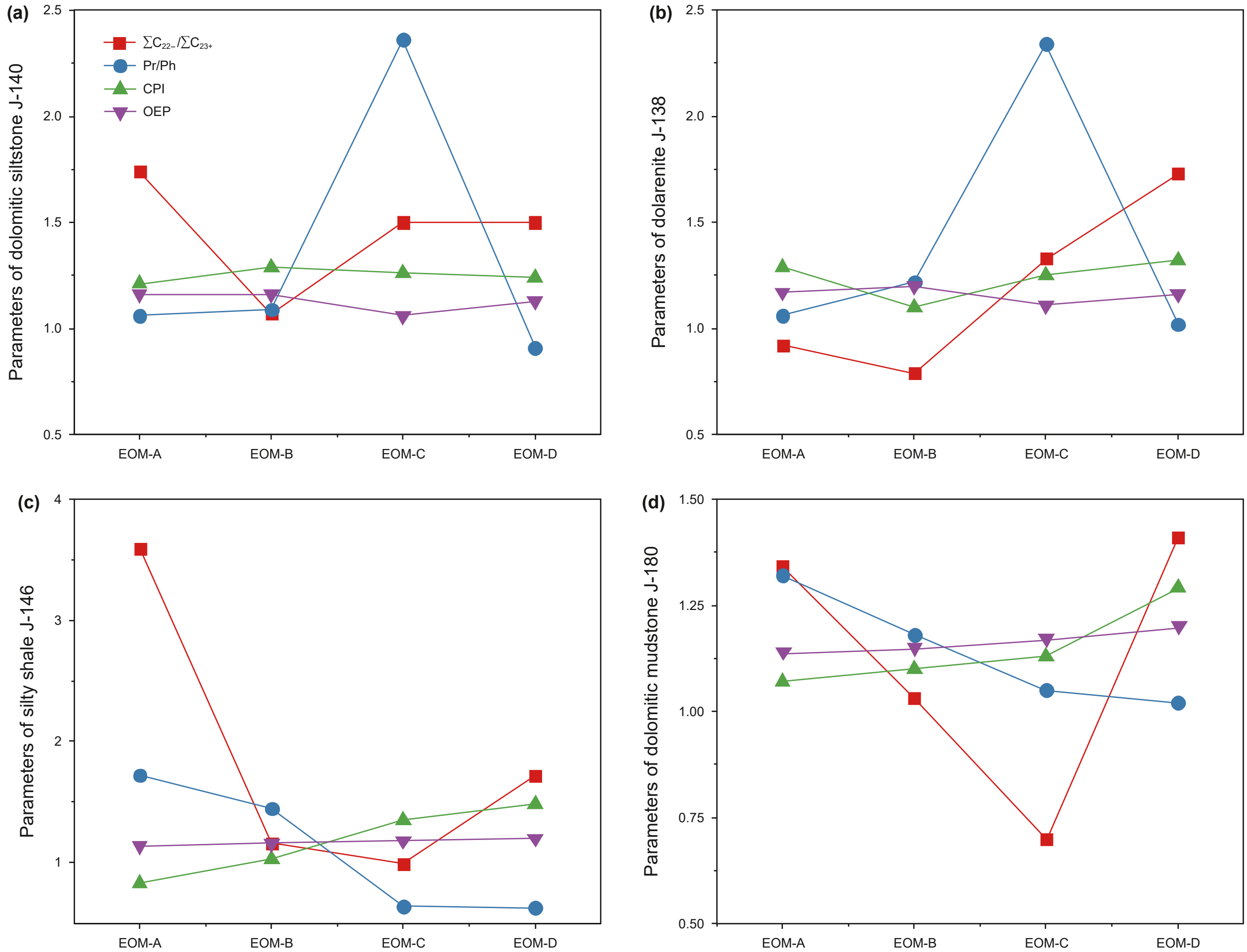

Fig. 12. Chromatographic parameters of saturated hydrocarbons in the four extracts from the four lithologies of the Lucaogou Formation, Jimusar Sag.

Table 4
Biomarker parameters of the terpanes and steranes in the four extracts from the four lithologies in the Lucaogou Formation, Jimusar Sag.

Lithology	Sample No.	Hydrocarbon of different occurrence states	$C_{24}TeT/C_{30}H$	Ga/αβC_{30}H	TT/Pt	T_s/T_m	C_{29}ββ/(ββ+αα)	C_{29}20S/(20S + 20R)
Dolomitic siltstone	J-140 (J10025, 3559.31 m)	EOM-A	0.05	0.16	0.19	0.12	0.36	0.44
		EOM-B	0.10	0.19	0.27	0.19	0.32	0.41
		EOM-C	0.12	0.20	0.20	0.23	0.37	0.47
		EOM-D	0.07	0.16	0.20	0.18	0.31	0.45
Dolarenite	J-138 (J10025, 3552.58 m)	EOM-A	0.06	0.16	0.17	0.12	0.32	0.41
		EOM-B	0.07	0.17	0.18	0.15	0.28	0.35
		EOM-C	0.07	0.19	0.21	0.22	0.34	0.45
		EOM-D	0.07	0.19	0.16	0.16	0.27	0.44
Silty shale	J-146 (J10025, 3575 m)	EOM-A	0.14	0.13	0.14	0.31	0.15	0.39
		EOM-B	0.06	0.18	0.16	0.27	0.16	0.38
		EOM-C	0.10	0.16	0.10	0.36	0.15	0.37
		EOM-D	0.06	0.10	0.04	0.23	0.12	0.33
Dolomitic mudstone	J-180 (J10025, 3709.19 m)	EOM-A	0.05	0.19	0.15	0.07	0.36	0.49
		EOM-B	0.03	0.19	0.15	0.06	0.35	0.41
		EOM-C	0.06	0.26	0.16	0.05	0.37	0.48
		EOM-D	0.07	0.29	0.10	0.04	0.35	0.46

Note: TT: Tricyclic terpane; Tet: Tetracyclic terpenes; H: Hopance; Ga: Gammacerane; Pt: Pentacyclic triterpane (Error margins of calculated biomarker parameters: ±0.005).

J-180 are significantly lower than those of the other three rock types, which may be related to the higher content of carbonate minerals or other factors. Because the T_s/T_m ratio is sensitive to clay-catalyzed reactions, the T_s/T_m ratio of oil derived from carbonate source rocks is low as compared with that derived from shale (Peters et al., 2004). In addition, the maturity parameter values of sterane in EOM-A to -D from the different lithologies do not change significantly (Table 4). However, the C_{29}20S(20S + 20R) and C_{29}αββ/(αββ + ααα) values of silty shale sample J-146 and dolomitic mudstone sample J-180 increase slightly from EOM-D to

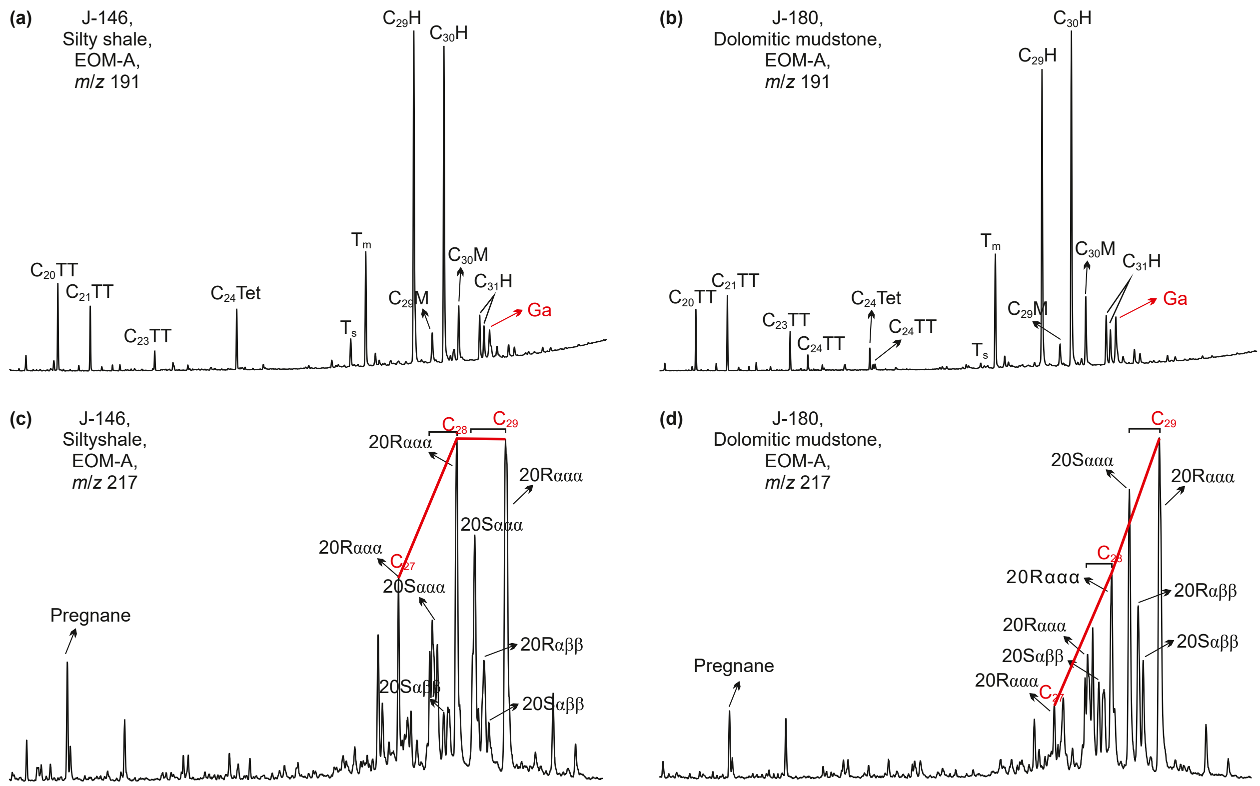

Fig. 13. Spectra of $m/z = 191$ terpanes and $m/z = 217$ steranes in EOM-A from the two types of mudstone in the Lucaogou Formation, Jimusar Sag.

-A (Table 4), indicative of a gradual increase in maturity. The two sterane maturity parameters for dolomitic siltstone sample J-140 and dolarenite sample J-138 vary slightly from EOM-D to -A (Table 4), again indicating that EOM-A and -B are migrated hydrocarbons.

5.4. *Shale oil potential and significance for resource evaluation*

5.4.1. *Occurrence state and shale oil potential*

Fig. 14 shows the distribution of group components in the four extracts from the nine samples of different lithologies. From EOM-A to -D, the proportion of saturated and aromatic hydrocarbons decreases, the total proportion of colloids and asphaltene increases, and the fluidity decreases gradually. For EOM-A and -B, almost all samples of EOM-B are richer in aromatics, colloids, and asphaltene than EOM-A (Figs. 9 and 14). Due to the relatively poor fluidity of colloidal and asphaltene components, and stronger adsorption onto mineral surfaces, they occur mainly in the matrix, and the mobility of EOM-B is weaker than that of EOM-A. Therefore, the lithologies with a higher proportion of EOM-A contain more available shale oil, which has some indicative significance for shale oil potential.

Pan et al. (2018) studied the occurrence state of retained hydrocarbons in shale source rocks in well Fan Ye 1 in the Dongying Sag, Bohai Bay Basin, and found that the saturated hydrocarbon contents of EOM-A were ~60%, while the asphaltene contents were <3%. In the Lucaogou Formation in the Jimusar Sag, samples of different lithologies all have high asphaltene contents (Fig. 14), with an average proportion of 40%. The group components in shale oil are all mixtures, precluding conversion into mole percentages; only the relative proportions of their absolute contents can be analyzed. It is necessary to be clarified that the Lucaogou Formation has an unusually high asphaltene component. The organic matter is in the stage of low-mature to mature so that the organic matter is not fully decomposed into light hydrocarbons, resulting in the products dominated by heavy components (colloids and asphaltenes). Also, it is related to the salt-tolerant algae such as Dunaliella, the special hydrocarbon parent material developed in this area (Wang et al., 2023). Due to its early hydrocarbon generation process, the content of heteroatoms in kerogen is high, which greatly reduces the average activation energy required for pyrolysis, resulting in the formation of crude oil at a low maturity stage and its quality is heavy. It contains more colloidal and asphaltene components than ordinary crude oil, and similar extraction results also exist in the Fengcheng Formation of Mahu Sag, Junggar Basin, in which the similar special hydrocarbon parent material also developed (Li et al., 2023; Xia et al., 2021). The Lucaogou Formation contains heavy oil, and thus a quantitative characterization of its occurrence state is important for shale oil exploration and development. With increasing extraction, the proportion of asphaltene increases (Fig. 14), and the average proportion of asphaltene in EOM-D is 54.11%. The saturated and aromatic hydrocarbon contents decrease gradually with increasing extraction (Fig. 14). In EOM-A, the average proportion of saturated hydrocarbons is 31.11%, the average proportion of aromatic hydrocarbons in EOM-B is 21.56%, and the average proportion of saturated hydrocarbon in EOM-D is reduced to 5.11% and the aromatic hydrocarbon is reduced to 2.78%. These results are related to the changes in the molecular composition of compounds in EOM-A to -D, and the overall increase in NSO compounds in the extracts.

In general, even if the lithologies are different, the same extracts have similar group compositions (Fig. 14), which indicate the chemical composition of soluble organic matter is closely related to its occurrence state. As such, the differences in the group compositions of the EOM types with different occurrence states reflect the controls of different lithologies, rock textures/

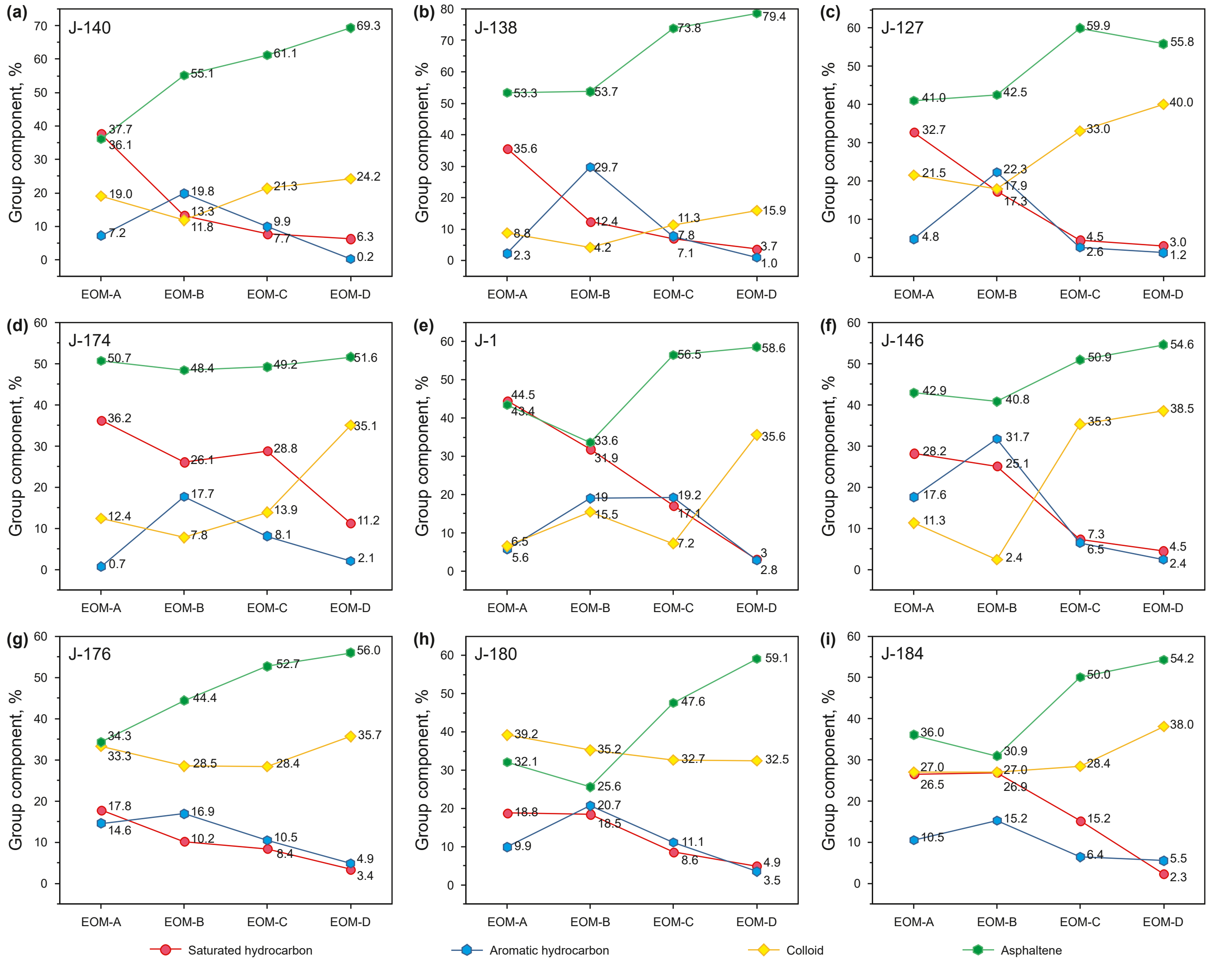

Fig. 14. Proportions of group components in the four extracts from the nine samples of different lithologies from the Lucaogou Formation, Jimusar Sag.

structures, and mineral types on organic matter enrichment (Wang and Cheng, 2000; Cai et al., 2007; Pan et al., 2018). Asphaltene and colloidal components have a strong polarity and high molecular weight, and readily bind with clay minerals or kerogen, and thus these two components form a large proportion of EOM-D (Mortland, 1970; Mayer, 1994; Cai et al., 2007). Yang et al. (2015) showed that carbonate minerals can readily adsorb colloidal components, while silicate minerals trap heavy components such as colloids and asphaltene. The macromolecular compounds in colloidal and asphaltene components often contain many polar groups, which are more easily combined with inorganic minerals or kerogen by ionic or hydrogen bonding than saturated and aromatic hydrocarbons. The saturated and aromatic hydrocarbons are mainly weakly polar or non-polar compounds, and occur mainly in the free or a weak physical adsorption state in EOM-A and -B. In summary, the main reasons for the decrease in fluidity of EOM-A, -B, -C, and -D are the gradual decrease in the saturated and aromatic hydrocarbon contents, and gradual increase in the contents of NSO compounds and asphaltenes.

The relative proportions of EOM-A and the proportions of total free components are positively correlated with OSI values, and the EOM-A contents and OSI values are higher in the siltstones and carbonate rocks (Fig. 15). This is because the contents of non-polar and weakly polar compounds in EOM-A are higher than those of hydrocarbons in the other occurrence states, and the fluidity is better, making the siltstones and carbonate rocks have better shale oil potential than the mudstones. As such, the occurrence state affects the microscopic shale oil flow and has some effect on the shale oil potential.

5.4.2. *Occurrence state modes of shale oil and implications for resource evaluation*

We established a model linking the lithology, rock density, and shale oil fluidity of the Lucaogou Formation, based on the evaluation results, the pore size distribution, and hydrocarbon generation and shale oil potential of the different lithofacies (Fig. 16). The NMR T_2 spectra show that the main pore throat size is >1 μm (Figs. 4 and 16) and, when the proportion of free oil is >70%, this corresponds to the high-quality sweet spots in siltstones and carbonate rocks that are similar to conventional reservoirs with coarse particles. The shale oil in these rocks is mainly in the free state and mobile, and flows according to Darcy's law (Pang et al., 2022; Jia et al., 2024). The proportion of free oil in the shale samples with bedding fractures and some shale samples with laminations that can effectively improve the filtration capacity can also be >50% (Figs. 5(b) and 6(c)–(d)). In these rocks, the pore throats are mainly about 10 nm to 1 μm in size (Figs. 4 and 16). In general, tight reservoirs are self-sealing and shale oil occurs in

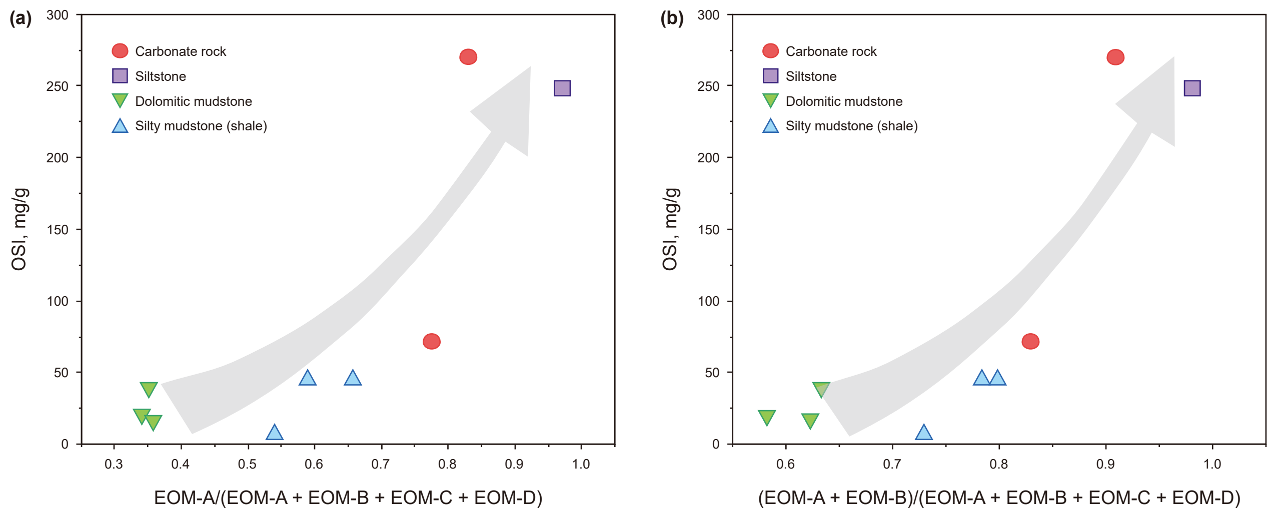

Fig. 15. Proportions of free hydrocarbons and OSI values in the sequential solvent extracts from the different lithologies of the Lucaogou Formation.

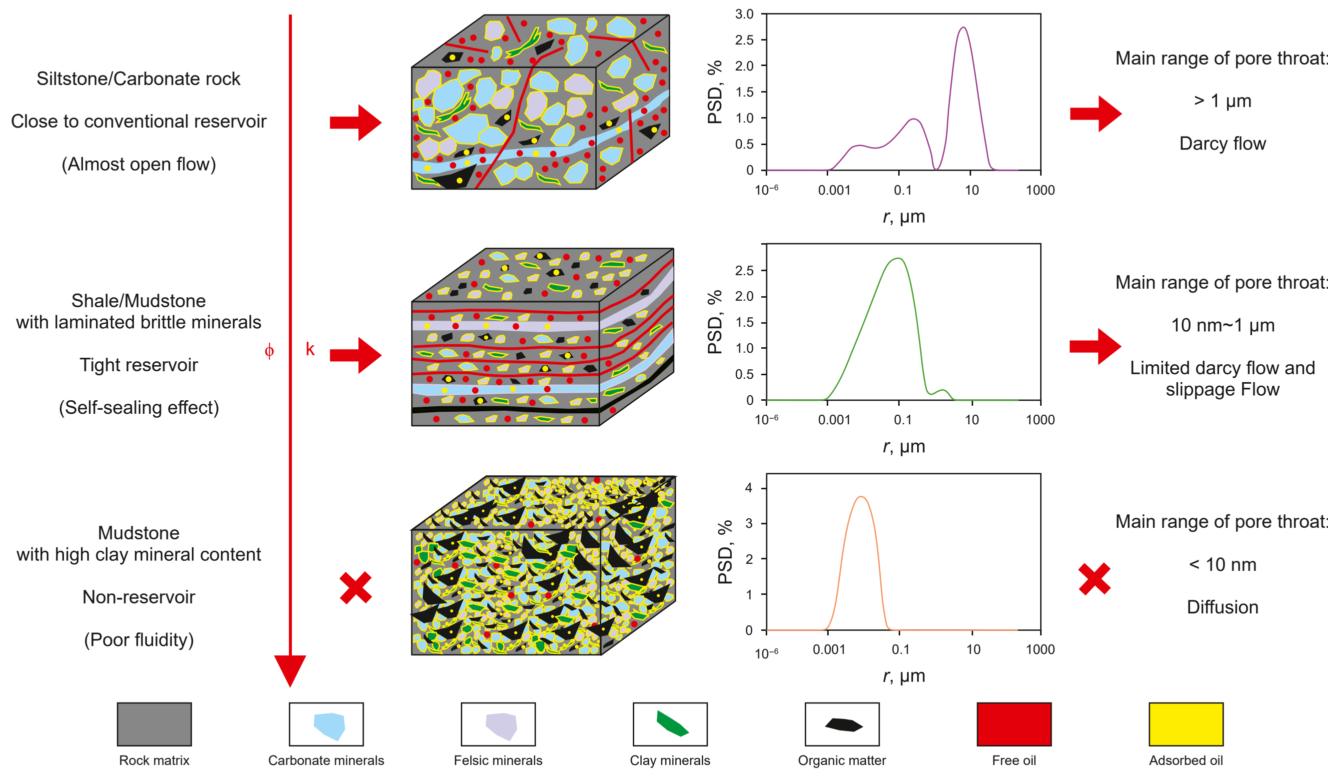

Fig. 16. Relationship between reservoir density and shale oil fluidity in the Lucaogou Formation.

both the free and adsorbed states, and undergoes both localized Darcy and multi-point slippage flow (Schowalter, 1979; Pang et al., 2022; Jia et al., 2024). For mudstones with a low content of brittle minerals and poor physical properties, the pore throats are mainly nanoscale (Figs. 4 and 16). In this case, adsorbed oil dominates (Figs. 5(b) and 6(e)) and the organic matter content is high. The large amount of adsorbed oil means the reservoir has a poor fluidity and the shale oil can only migrate slowly by diffusion to near-source rocks with good permeability (Song et al., 2021; Pang et al., 2022; Jia et al., 2024).

For shale oil resource evaluation, the amount of conventional EOM extracted by the Soxhlet technique and the rock pyrolysis S_1 value are commonly used as basic parameters for resource calculations. However, the sequential solvent extraction technique can determine the contents of different types of free and adsorbed hydrocarbons, and can directly characterize the chemical compositions of organic matter in different occurrence states at the molecular level. Solvent extraction cannot completely separate soluble organic matter with different occurrence states, and the occurrence state of soluble organic matter in rocks also has a certain dynamic transformation process, and changes in the solvent and extraction methodology can also affect the results. But the general geological laws are right. In summary, EOM-A obtained by sequential solvent extraction has the highest fluidity. Given that isolated pores in a sample are opened to solvents during crushing, this process is similar to hydraulic fracturing during shale oil production (Tamimi and Uysal, 1990), and thus EOM-B can represent the oil production capacity after hydraulic fracturing, and also has some mobility. Dolomitic mudstone with high EOM-B content may demonstrates significant potential for enhancing shale oil productivity after fracturing. For instance, in the Permian Basin of the U.S., certain dolomitic mudstone intervals achieved over 40% increase in initial production by adopting "close-spaced fracturing" techniques (combining high-density perforation clusters with short interval spacing) to elevate fracture density. High dolomite content may enhance rock brittleness, facilitating primary fracture propagation, yet the presence of clay minerals (e.g., illite) risks compromising fracture conductivity over time. This necessitates optimizing chemical property of fracturing fluid, such as incorporating clay stabilizers (Curtis, 2002; Ko et al., 2017; Wang et al., 2019). In general, while dolomitic mudstone exhibits moderate porosity and permeability even with high EOM-B content, fracturing strategies must be customized to its mineralogy and mechanical properties, balancing upfront costs against long-term gains. Advancements in stimulation technology may position such reservoirs as a critical supplement to unconventional resource development. Although EOM-C and -D are theoretically immobile hydrocarbons during normal production and hydraulic fracturing, their mobility and productivity could be improved with future advances in production technology. Compared to global shale systems, U.S. marine shales generally feature organic pores and microfractures as dominant storage spaces, with superior pore connectivity and permeability (e.g., Matrix permeability in Eagle Ford reaches 1100 mD). Their high carbonate mineral content (e.g., 40% in Eagle Ford) enhances fracture conductivity (Curtis, 2002; Ko et al., 2017). In contrast, Chinese lacustrine shales, like the Lucaogou Formation, primarily rely on inorganic pores (intercrystalline and cracks between clay layers) with poorly developed organic pores, complex pore size distributions, poor connectivity, and permeability typically below 100 mD, necessitating artificial stimulation via hydraulic fracturing. The Eagle Ford shale achieves high production through a source-reservoir integration model (organic-rich shale interbedded with carbonate interlayers), where high carbonate content (>40%) and low clay minerals (8%) provide ideal fracturing conditions (Ko et al., 2017; Wang et al., 2019). For lacustrine shales in China, it should be focused on targeting sweet spots such as carbonate, siltstone interbeds, and dolomitic mudstone, while developing geological engineering integration technologies. This includes optimizing horizontal well trajectories (prioritizing thin sandstone layers or fracture zones) and formulating nano-modified fracturing fluids to enhance proppant transport.

In the exploration and development of lacustrine shale oil, different lithologies (e.g., dolomitic mudstones vs. siltstones) may require specific hydraulic fracturing techniques tailored to their characteristics. For instance, dolomitic mudstones typically exhibit high plasticity and low strength, and their fracture propagation may be influenced by strata plasticity, necessitating fracturing techniques capable of overcoming this plasticity. This might involve employing higher fracturing fluid injection rates or optimized fluid formulations to create effective fracture networks (Ko et al., 2017). Siltstones, characterized by higher strength and better brittleness, may allow for more straightforward and controllable fracture propagation. And more flexible and efficient fracturing methods such as multi-stage fracturing or water fracturing could be applied. It should be noted that field operations must integrate parameters including in-situ stress, brittleness, and the degree of natural fracture development, with experimental and simulation-based optimization of technical combinations to achieve cost-effective reservoir stimulation.

6. Conclusions

We investigated the occurrence states and contents of lacustrine shale oil in the Lucaogou Formation. The free oil forms the basis of shale oil production and the adsorbed oil represents potential future shale oil production capacity. The Lucaogou Formation contains low-mature to mature shale with a good heavy oil content, and the occurrence state of the shale oil affects its fluidity, which is an important control on the shale oil enrichment and productivity.

In the Lucaogou Formation, siltstones and carbonate rocks form the high-quality sweet spots with the best shale oil fluidity. Shales with well-developed bedding fractures or laminated mineral layers also contain available shale oil in the free state. After fracturing, the shale oil productivity of the dolomitic mudstone can be increased. The free oil contents in reservoirs such as carbonate rocks and siltstones are more affected by physical properties, but the free oil contents in mudstones are also controlled by the TOC contents and maturity. The adsorbed oil contents in all the lithologies are mainly affected by TOC contents. The biomarkers in the extracts revealed that the siltstones and carbonate rocks contain migrated hydrocarbons, and the maturity of the adsorbed hydrocarbons in all the rocks is lower than that of the free hydrocarbons. EOM-A and -D are more likely to adsorb some weakly polar or non-polar molecules. Saturated hydrocarbons have higher $\sum C_{22-}/\sum C_{23+}$ values, and the $\sum C_{22-}/\sum C_{23+}$ values of saturated hydrocarbons in EOM-C are the lowest because carbonate minerals tend to include early formed, long-chain *n*-alkanes. In summary, for shale oil in mixed sedimentary strata in saline lacustrine basin, variable lithofacies makes the occurrence state of soluble organic matter obviously different. The occurrence state affects the shale oil fluidity from a microscopic perspective. Future exploration and production should also consider the shale oil occurrence state combined with favorable lithologies, which might provide a more robust guide for the identification of potential sweet spots. This study will also have implications for the occurrence state and enrichment mechanism of shale oil in other saline lacustrine basins with similar mixed sedimentary lithofacies.

It is worth mentioning that the sequential extraction method can gerally characterize the contents of soluble organic matter with different maturities or occurrence states in variable lithologies, and can directly characterize the chemical compositions of organic matter in different occurrence states at the molecular level. But the procedure is complex and time-consuming, and thus it is only applicable to a small number of samples. And oil in micropores, adsorbed on kerogen surfaces, or within swollen/dissolved states exhibits stronger polarity, lower accessibility, or negligible abundance, rendering Soxhlet extraction ineffective for these fractions. In addition, there may be a single well sampling bias (J10025) in this study, and multi-well analyses can be performed in future work. Also, future studies may further optimize solvent combinations and extraction sequences to better reflect the complexity of actual subsurface oil compositions. More solvent combinations can be used to simulate real reservoir conditions, and in combination with supercritical fluid extraction technology to improve extraction efficiency. It can also be combined with molecular dynamics simulation technology, which is expected to reveal the dynamic processes of oil-rock interactions at the microscopic scale.

CRediT authorship contribution statement

Chen-Jia Zhang: Conceptualization, Methodology, Writing – original draft, Formal analysis, Data curation, Software. **Jian Cao:** Writing – review & editing, Conceptualization, Funding

acquisition, Supervision. **Bao-Li Xiang:** Project administration, Resources. **Bao-Jian Shen:** Investigation, Methodology, Validation. **Ni Zhou:** Resources, Project administration, Funding acquisition. **Wen-Yao Xiao:** Methodology, Software, Formal analysis. **Yan Wang:** Methodology, Software. **Yu-Ce Wang:** Resources, Validation. **Xu-Sheng Guo:** Supervision, Funding acquisition, Conceptualization, Investigation.

Declaration of competing interest

The authors declare that they have no known competing financial interests or personal relationships that could have appeared to influence the work reported in this paper.

Acknowledgements

We thank editors, and anonymous reviewers for their insightful comments and suggestions in improving the manuscript. This work was jointly funded by the National Natural Science Foundation of China (Grant Nos. 42230808 and 41830425) and PetroChina Science and Technology Major Project (Grant No. 2021DJ0108).

References

Allen, M., Natal' in, B., 1995. Junggar, Turfan and Alakol basins as late Permian to Early Triassic extensional structures in a sinistral shear zone in the Altaid orogenic collage, Central Asia. J. Geol. Soc. 152 (2), 327–338. https://doi.org/10.1144/gsjgs.152.2.0327.

Amijaya, H., Littke, R., 2006. Properties of thermally metamorphosed coal from Tanjung Enim Area, South Sumatra Basin, Indonesia with special reference to the coalification path of macerals. Int. J. Coal Geol. 66, 271–295. https://doi.org/10.1016/j.coal.2005.07.008.

Birdwell, J.E., Washburn, K.E., 2015. Multivariate analysis relating oil shale geochemical properties to NMR relaxometry. Energy & Fuels 29, 2234–2243. https://doi.org/10.1021/ef502828k.

Cai, J.G., Bao, Y.J., Yang, S.Y., et al., 2007. Research on preservation and enrichment mechanisms of organic matter in muddy sediment and mudstone. Sci. China E 37 (2), 234–243. https://doi.org/10.1007/s11430-007-0005-0 (in Chinese).

Cao, Z., Liu, G.D., Zhan, H.B., et al., 2016. Geological control factors of micro oil distribution in tight reservoirs. Mar. Petrol. Geol. 77, 1193–1205. https://doi.org/10.1016/j.marpetgeo.2016.08.013.

Cardott, B.J., 2012. Thermal maturity of woodford shale gas and oil plays, Oklahoma, USA. Int. J. Coal Geol. 103, 109–119. https://doi.org/10.1016/j.coal.2012.06.004.

Curtis, J.B., 2002. Fractured shale-gas systems. AAPG Bull. 86 (11), 1921–1938. https://doi.org/10.1306/61EEDDBE-173E-11D7-8645000102C1865D.

Dickey, J.S., 1975. A hypothesis of origin for podiform chromite deposits. Geochem. Cosmochim. Acta 39 (6–7), 1061–1062. https://doi.org/10.1016/B978-0-08-019954-2.50026-3.

Falegnami, A., Tomassi, A., Corbelli, G., et al., 2024a. Managing complexity in socio-technical systems by mimicking emergent simplicities in nature: A brief communication. Biomimetics 9 (6), 322. https://doi.org/10.3390/biomimetics9060322.

Falegnami, A., Tomassi, A., Gunella, C., et al., 2024b. Defining conceptual artefacts to manage and design simplicities in complex adaptive systems. Heliyon 10 (24), e41033. https://doi.org/10.1016/j.heliyon.2024.e41033.

Fang, S., Song, Y., Xu, H., et al., 2007. Relationship between tectonic evolution and petroleum system formation-taking the Jimusar sag of Eastern Junggar basin as an example. Petrol. Geol. & Exp. 29 (2), 149–154. https://doi.org/10.11781/sysydz200702149 (in Chinese).

Guan, P., Xu, Y.C., Liu, W.H., 1998. Different occurrence states and quantitative estimation of organic matter in source rocks. Chin. Sci. Bull. 43 (14), 1556–1559 (in Chinese).

Hu, T., Pang, X.Q., Jiang, S., et al., 2018. Oil content evaluation of lacustrine organic-rich shale with strong heterogeneity: A case study of the middle Permian Lucaogou formation in Jimusaer sag, Junggar Basin, NW China. Fuel 221, 196–205. https://doi.org/10.1016/j.fuel.2018.02.082.

Hu, T., Pang, X.Q., Jiang, F.J., et al., 2021. Movable oil content evaluation of lacustrine organic-rich shales: Methods and a novel quantitative evaluation model. Earth Sci. Rev., 103545 https://doi.org/10.1038/sj.cr.7290029.

Huang, Z.K., Hao, Y.Q., Li, S.J., et al., 2020. Oil-bearing potential, mobility evaluation and significance of shale oil in Chang 7 shale system in the Ordos Basin: A case study of well H317. Geol. in China. 47 (1), 210–219. https://doi.org/10.12029/gc20200117 (in Chinese).

Jarvie, D.M., 2012. Shale resource systems for oil and gas: part 2-Shale-oil resource systems. Breyer, J.A. (Ed.), Shale reservoirs-giant Resources for the 21st Century. AAPG Bull, vol. 97, pp. 89–119. https://doi.org/10.1306/13321447M973489.

Jarvie, D.M., Hill, R.J., Ruble, T.E., et al., 2007. Unconventional shale-gas systems: the Mississippian Barnett shale of north-central Texas as one model for thermogenic shale-gas assessment. AAPG Bull. 91 (4), 475–499. https://doi.org/10.1306/12190606068.

Jia, C.Z., Pang, X.Q., Song, Y., 2024. Basic principles of the whole petroleum system. Petrol. Explor. Dev. 51 (4), 679–691. https://doi.org/10.1016/s1876-3804(24)60506-9.

Jiang, Y.Q., Liu, Y.Q., Yang, Z., et al., 2015. Characteristics and origin of tuff-type tight oil in Jimusar depression, Junggar Basin, NW China. Petrol. Explor. Dev. 42 (6), 741–749. https://doi.org/10.11698/PED.2015.06.06.

Jiang, Q.G., Li, M.W., Qian, M.H., et al., 2016. Quantitative characterization of shale oil in different occurrence states and its application. Pet. Geol. & Expe. 38 (6), 842–849. https://doi.org/10.11781/sysydz201606842 (in Chinese).

Jiang, Z.X., Li, T.W., Gong, H.J., et al., 2020. Characteristics of low-mature shale reservoirs in Zhanhua sag and their influence on the mobility of shale oil. Acta Petrol. Sin. 41 (2), 1587–1600. https://doi.org/10.7623/syxb202012011.

Jiao, X., Liu, Y.Q., Yang, W., 2023. Microcrystalline dolomite in a middle Permian volcanic lake: insights on primary dolomite formation in a non-evaporitic environment. Sedimentology 70, 48–77. https://doi.org/10.1111/sed.13031.

Khorasani, G.K., 1987. Novel development in fluorescence microscopy of complex organic mixtures:application in petroleum geochemistry. Org. Geochem. 11 (3), 157–168. https://doi.org/10.1016/0146-6380(87)90019-2.

Ko, L.T., Loucks, R.G., Ruppel, S.C., et al., 2017. Origin and characterization of Eagle ford pore networks in the south Texas Upper Cretaceous shelf. AAPG Bull. 101 (3), 387–418. https://doi.org/10.1306/08051616035.

Koopmans, M.P., Rijpstra, W.I., Klapwijk, M., et al., 1999. A thermal and chemical degradation approach to decipher pristane and phytane precursors in sedimentary organic matter. Org. Geochem. 30 (9), 1089–1104. https://doi.org/10.1016/S0146-6380(99)00088-1.

Kuang, L.C., Tang, Y., Lei, D.W., et al., 2012. Formation conditions and exploration potential of tight oil in the Permian saline lacustrine dolomitic rock, Junggar basin, NW China. Petrol. Explor. Dev. 39 (6), 657–667. https://doi.org/10.1016/S1876-3804(12)60095-0.

Kus, J., Araujo, C.V., Borrego, A.G., et al., 2017. Identification of alginite and bituminite in rocks other than coal. 2006, 2009, and 2011 round robin exercises of the ICCP identification of dispersed organic matter working group. Int. J. Coal Geol. 178, 26–38. https://doi.org/10.1016/j.coal.2017.04.013.

Larter, S.R., Huang, H.P., Snowdon, L., et al., 2012. What we do not know about self-sourced oil reservoirs: challenges and potential solutions. In: SPE 162777, pp. 1–4. https://doi.org/10.2118/162777-MS.

Li, Z., 2020. Comparison of oil-bearing properties and oil mobility of shale with different lithologies in Continental basins: a case study of the upper fourth member of Paleogene Shahejie formation in Dongying Sag, Bohai Bay Basin. Petrol. Geol. & Exp. 42, 545–595. https://doi.org/10.11781/sysydz202004545.

Li, Z., Zou, Y.R., Xu, X.Y., et al., 2016. Adsorption of mudstone source rock for shale oil – experiments, model and a case study. Org. Geochem. 92, 55–62. https://doi.org/10.1016/j.orggeochem.2015.12.009.

Li, S.T., Li, S.X., Guo, R.L., 2021. Occurrence state of soluble organic matter in shale oil reservoirs from the Upper Triassic Yanchang formation in the Ordos Basin, China: insights from multipolarity sequential extraction. Nat Resour Res 30, 4379–4402. https://doi.org/10.1007/s11053-021-09959-6.

Li, J.B., Jiang, C.Q., Wang, M., et al., 2022. Determination of in situ hydrocarbon contents in shale oil plays. Part 1: is routine Rock–Eval analysis reliable for quantifying the hydrocarbon contents of preserved shale cores? Org. Geochem. 170, 104449. https://doi.org/10.1016/j.orggeochem.2022.104449.

Li, W.W., Cao, J., Hu, W.X., et al., 2023. Revealing continuous hydrocarbon generation and shale oil accumulation of saline lacustrine source rocks by sequential extraction. Fuel 352, 129081. https://doi.org/10.1016/j.fuel.2023.129081.

Liu, H.M., Zhang, S., Bao, Y.S., et al., 2019. Geological characteristics and effectiveness of the shale oil reservoir in Dongying sag. Oil Gas Geol. 40 (3), 512–523. https://doi.org/10.11743/ogg20190307.

Lu, S.F., Huang, W.B., Chen, F.W., et al., 2012. Classification and evaluation criteria of shale oil and gas resources: discussion and application. Pet. Explor. Dev. 39, 268–276. https://doi.org/10.1016/S1876-3804(12)60042-1.

Mayer, L.M., 1994. Surface area control of organic carbon accumulation in continental shelf sediments. Geochem. Cosmochim. Acta 58 (4), 1271–1284. https://doi.org/10.1016/0016-7037(94)90381-6.

Mei, B.W., Liu, X.J., 1980. The distribution of isoprenoid alkanes in China's crude oil and its relation with the geologic environment. Oil Gas Geol. 1 (2), 99–115. https://doi.org/10.11743/ogg19800203 (in Chinese).

Mortland, M.M., 1970. Clay-organic complexes and interactions. Adv. Agron. 22, 75–117. https://doi.org/10.1016/s0065-2113(08)60266-7.

Ning, C.X., Ma, Z.L., Jiang, Z.X., et al., 2020. Effect of shale Reservoir characteristics on shale oil movability in the lower third member of the Shahejie formation, Zhanhua sag. Acta Geol. Sin. 94 (2), 352–363. https://doi.org/10.1111/1755-6724.14284.

Olariu, C., Zhang, Z.J., Zhou, C.M., et al., 2022. Conglomerate to mudstone lacustrine cycles revealed in Junggar Basin, Northwest China: Middle Permian Lucaogou and Jingjingzigou formations. Mar. Petrol. Geol. 136, 105473. https://doi.org/10.1016/j.marpetgeo.2021.105473.

Pan, C.C., Liu, D.Y., 2009. Molecular correlation of free oil, adsorbed oil and inclusion oil of reservoir rocks in the Tazhong Uplift of the Tarim basin, China. Org. Geochem. 40, 387–399. https://doi.org/10.1016/j.orggeochem.2008.11.005.

Pan, Y.H., Li, M.W., Sun, Y.G., et al., 2018. Geochemical characterization of soluble organic matter with different existing states in low-maturity argillaceous source rocks of lacustrine facies. Geochimica 47 (4), 335–344. https://doi.org/10.19700/j.0379-1726.2018.04.002 (in Chinese).
Pang, X.Q., Jia, C.Z., Song, Y., et al., 2022. Quantitative evaluation of whole petroleum system: principle and application. Acta Petrol. Sin. 43 (6), 727–759. https://doi.org/10.7623/syxb202206001 (in Chinese).
Peters, K.E., 1986. Guidelines for evaluating petroleum source rock using programmed pyrolysis. AAPG Bull. 70 (3), 318–329. https://doi.org/10.1306/94885688-1704-11D7-8645000102C1865D.
Peters, K.E., Walters, C.C., Moldowan, J.M., 2004. The Biomarker Guide: Column 2, Biomarkers and Isotopes in Petroleum Systems and Earth History, second ed. Cambridge University Press, Cambridge, pp. 475–625. https://doi.org/10.1017/CBO9780511524868.
Pickel, W., Kus, J., Flores, D., et al., 2017. Classification of liptinite–ICCP system 1994. Int. J. Coal Geol. 169, 40–61. https://doi.org/10.1016/j.coal.2016.11.004.
Qian, M.H., Jiang, Q.G., Li, M.W., et al., 2017. Quantitative characterization of extractable organic matter in lacustrine shale with different occurrences. Pet. Geol. & Expe. 39 (2), 278–286. https://doi.org/10.11781/sysydz201702278 (in Chinese).
Qiu, Z., Shi, Z.S., Dong, D.Z., et al., 2016. Geological characteristics of source rock and reservoir of tight oil and its accumulation mechanism: a case study of Permian Lucaogou formation in Jimusar sag, Junggar basin. Petrol. Explor. Dev. 43 (6), 928–939. https://doi.org/10.1016/S1876-3804(16)30118-5.
Raji, M., Gröcke, D.R., Greenwell, H.C., et al., 2015. The effect of interbedding on shale reservoir properties. Mar. Petrol. Geol. 67, 154–169. https://doi.org/10.1016/j.marpetgeo.2015.04.015.
Romero-Sarmiento, M.F., 2019. A quick analytical approach to estimate both free versus sorbed hydrocarbon contents in liquid-rich source rocks. AAPG Bull. 103, 2031–2043. https://doi.org/10.1306/02151918152.
Sanei, H., Wood, J.M., Ardakani, O.H., et al., 2015. Characterization of organic matter fractions in an unconventional tight gas siltstone reservoir. Int. J. Coal Geol. 150–151, 296–305. https://doi.org/10.1016/j.coal.2015.04.004.
Schowalter, T.T., 1979. Mechanics of secondary hydrocarbon migration and entrapment. AAPG Bull. 63 (5), 723–760. https://doi.org/10.1306/2F9182CA-16CE-11D7-8645000102C1865D.
Song, Y.Q., Kausik, R., 2019. NMR application in unconventional shale Reservoirs–A new porous media research frontier. Prog. Nucl. Magn. Reson. Spectrosc. 112–113, 17–33. https://doi.org/10.1016/j.pnmrs.2019.03.002.
Song, L.P., Xue, H.T., Lu, S.F., et al., 2015. The research progress on the occurrence mechanism of detained hydrocarbon. Acta Geol. Sin. 89 (S1), 164–165. https://doi.org/10.1111/1755-6724.12303_6.
Song, Y., Luo, Q., Jiang, Z.X., et al., 2021. Enrichment of tight oil and its controlling factors in central and western China. Petrol. Explor. Dev. 48 (2), 421–433. https://doi.org/10.1016/S1876-3804(21)60040-X.
Spiro, B., 1984. Effects of the mineral matrix on the distribution of geochemical markers in thermally affected sedimentary sequences. Org. Geochem. 6, 543–559. https://doi.org/10.1016/0146-6380(84)90077-9.
Su, S.Y., Jiang, Z.X., Shan, X.L., et al., 2018. The effects of shale pore structure and mineral components on shale oil accumulation in the Zhanhua Sag, Jiyang Depression, Bohai Bay Basin, China. J. Pet. Sci. Eng. 165, 365–374. https://doi.org/10.1016/j.petrol.2018.02.030.
Tamimi, A., Uysal, B.Z., 1990. Parametric investigation of oil-shale extraction with organic solvents. Sep. Sci. 25 (10), 1151–1159. https://doi.org/10.1080/01496399008051844.
Tang, X., Zhang, J.C., Wang, X.Z., et al., 2014. Shale characteristics in the southeastern ordos basin, China: implications for hydrocarbon accumulation conditions and the potential of continental shales. Int. J. Coal Geol. 128–129, 32–46. https://doi.org/10.1016/J.COAL.2014.03.005.
Tomassi, A., Trippetta, F., de Franco, R., et al., 2022. From petrophysical properties to forward-seismic modeling of facies heterogeneity in the carbonate realm (Majella Massif, central Italy). J. Petrol. Sci. Eng. 211, 110242. https://doi.org/10.1016/j.petrol.2022.110242.
Tomassi, A., de Franco, R., Trippetta, F., 2024. High-resolution synthetic seismic modelling: elucidating facies heterogeneity in carbonate ramp systems. Pet. Geosci. 31, 2024–2047. https://doi.org/10.1144/petgeo2024-047.
Uffmann, A.K., Littke, R., Rippen, D., 2012. Mineralogy and geochemistry of Mississippian and Lower Pennsylvanian black shales at the Northern margin of the Variscan Mountain belt (Germany and Belgium). Int. J. Coal Geol. 103, 92–108. https://doi.org/10.1016/j.coal.2012.08.001.
U.S. EIA, 2013. Technically Recoverable Shale Oil and Shale Gas Resources: an Assessment of 137 Shale Formation in 41 Countries Outside the United States. Washington. https://www.eia.gov/.
Wang, Z.Y., Cheng, K.M., 2000. The organic geochemical characteristics comparison and contributors of different existing state organic matter in carbonate rocks. Acta Sedimentol. Sin. 18 (4), 600–605. https://doi.org/10.14027/j.cnki.cjxb.2000.04.021 (in Chinese).
Wang, S., Feng, Q.H., Zha, M., et al., 2015. Molecular dynamics simulation of liquid alkane occurrence state in pores and slits of shale organic matter. Petrol. Explor. Dev. 42 (6), 844–851. https://doi.org/10.1016/S1876-3804(15)30081-1.
Wang, M., Ma, R., Li, J.B., et al., 2019. Occurrence mechanism of lacustrine shale oil in the Paleogene shahejie formation of Jiyang depression, Bohai Bay Basin, China. Petrol. Explor. Dev. 46 (4), 833–846. https://doi.org/10.1016/S1876-3804(19)60242-9.
Wang, E.Z., Feng, Y., Guo, T.L., et al., 2022a. Oil content and resource quality evaluation methods for lacustrine shale: A review and a novel three-dimensional quality evaluation model. Earth Sci. Rev. 232, 104134. https://doi.org/10.1016/j.earscirev.2022.104134.
Wang, M., Li, M., Li, J.B., et al., 2022b. The key parameter of shale oil resource evaluation: oil content. Pet. Sci. 19, 1443–1459. https://doi.org/10.1016/j.petsci.2022.03.006.
Wang, Y.C., Cao, J., Tao, K.Y., et al., 2023. Origin of heavy shale oil in saline lacustrine basins: Insights from the Permian Lucaogou Formation, Junggar Basin. AAPG Bull. 107 (9), 1553–1579. https://doi.org/10.1306/10242222027.
Wei, L., Mastalerz, M., Schimmelmann, A., et al., 2014. Influence of Soxhlet-extractable bitumen and oil on porosity in thermally maturing organic-rich shales. Int. J. Coal Geol. 132, 38–50. https://doi.org/10.1016/j.coal.2014.08.003.
Wu, H.G., Hu, W.X., Wang, Y.C., et al., 2021. Depositional conditions and accumulation models of tight oils in the middle Permian Lucaogou formation in Junggar Basin, northwestern China: New insights from geochemical analysis. AAPG Bull. 105 (12), 2477–2518. https://doi.org/10.1306/06222118094.
Xia, L.W., Cao, J., Hu, W.X., Zhi, D.M., Tang, Y., Li, E.T., He, W.J., 2021. Coupling of paleoenvironment and biogeochemistry of deep-time alkaline lakes: A lipid biomarker perspective. Earth Sci. Rev. 213, 103499. https://doi.org/10.1016/j.earscirev.2020.103499.
Xiao, W.J., Han, C.M., Yuan, C., et al., 2008. Middle Cambrian to Permian subduction-related accretionary orogenesis of northern Xinjiang, NW China: implications for the tectonic evolution of central Asia. J. Asian Earth Sci. 32 (2–4), 102–117. https://doi.org/10.1016/j.jseaes.2007.10.008.
Xiao, W.Y., Cao, J., Luo, B., et al., 2023. Recovering original type and abundance of organic matter in spent source rocks: A review and advances in elemental proxies. AAPG Bull. 107 (2), 243–281. https://doi.org/10.1306/09282221129.
Xie, X.M., Li, M.W., Littke, R., et al., 2016. Petrographic and geochemical characterization of microfacies in a lacustrine shale oil system in the Dongying Sag, Jiyang depression, Bohai Bay Basin, eastern China. Int. J. Coal Geol. 165, 49–63. https://doi.org/10.1016/j.coal.2016.07.004.
Yang, Y., Lei, T.Z., Guan, B.W., et al., 2015. Differences of solvable organic matters with different occurrence states in argillaceous source rocks of coastal shallow-lake facie. Lithologic reservoirs. Lit. Res. 27 (2), 77–82. https://doi.org/10.3969/j.issn.1673-8926.2015.02.012 (in Chinese).
Zhang, L.Y., Bao, Y.S., Li, J.Y., et al., 2014. Movability of lacustrine shale oil: A case study of Dongying Sag, Jiyang Depression, Bohai Bay Basin. Petrol. Explor. Dev. 41 (6), 641–649. https://doi.org/10.1016/S1876-3804(14)60084-7.
Zhang, S.M., Cao, Y.C., Liu, K.Y., et al., 2018. Characterization of lacustrine mixed fine-grained sedimentary rocks using coupled chemostratigraphic-petrographic analysis: a case study from a tight oil reservoir in the Jimusar Sag, Junggar Basin. Mar. Petrol. Geol. 99, 453–472. https://doi.org/10.1016/j.marpetgeo.2018.10.039.
Zhang, H.J., Chen, Y., Wang, M., et al., 2019a. Quantitative determination of the proportion of mixed crude oil with different maturity by fluorescence spectra: take a case of the ES_4 oil in the Dongying depression. Spectrosc. Spectr. Anal. 39 (11), 3414–3419. https://doi.org/10.3964/j.issn.1000-0593(2019)11-3414-06.
Zhang, J.Y., Liu, G.D., Cao, Z., et al., 2019b. Characteristics and formation mechanism of multi-source mixed sedimentary rocks in a saline lake, a case study of the Permian Lucaogou Formation in the Jimusaer sag, northwest China. Mar. Petrol. Geol. 102, 704–724. https://doi.org/10.1016/j.marpetgeo.2019.01.016.
Zhang, H., Huang, H.P., Li, Z., et al., 2020. Comparative study between sequential solvent-extraction and multiple isothermal stages pyrolysis: A case study on Eocene Shahejie formation shales, Dongying depression, East China. Fuel 263, 116591. https://doi.org/10.1016/j.fuel.2019.116591.
Zhang, C.J., Cao, J., Li, E.T., et al., 2021. Revisiting controls on shale oil accumulation in saline lacustrine basins: the Permian lucaogou formation mixed rocks, Junggar Basin. Geofluids 3, 1–25. https://doi.org/10.1155/2021/5206381.
Zhang, C.J., Cao, J., Xiang, B.L., et al., 2023. Occurrence state of shale oil in saline lacustrine basins: a lithofacies perspective. J. Asian Earth Sci. 255, 105799. https://doi.org/10.1016/j.jseaes.2023.105799.
Zhao, W.Z., Hu, S.Y., Hou, L.H., et al., 2020. Types and resource potential of continental shale oil in China and its boundary with tight oil. Petrol. Explor. Dev. 47 (1), 1–10. https://doi.org/10.1016/S1876-3804(20)60001-5.
Zhao, W.Z., Zhang, B., Wang, X.M., et al., 2021. Differences in source kitchens for lacustrine in-source and out-source hydrocarbon accumulations onshore China. Petrol. Explor. Dev. 48 (3), 1–12. https://doi.org/10.11698/PED.2021.03.03.
Zhi, D.M., Tang, Y., Yang, Z.F., et al., 2019. Geological characteristics and accumulation mechanism of continental shale oil in Jimusaer Sag, Junggar Basin. Oil Gas Geol. 40 (3), 524–534. https://doi.org/10.11743/ogg20190308 (in Chinese).
Zhi, D.M., Xiang, B.L., Zhou, N., et al., 2023. Contrasting shale oil accumulation in the upper and lower sweet spots of the lacustrine Permian Lucaogou Formation, Junggar Basin. China. Mar. Petrol. Geol. 150, 106178. https://doi.org/10.1016/j.marpetgeo.2023.106178.
Zou, C.N., Yang, Z., Zhu, R., et al., 2015. Progress in China's unconventional oil & gas exploration and development and theoretical technologies. Acta Geol. Sin. 89 (3), 938–971. https://doi.org/10.1111/1755-6724.12491.
Zou, C.N., Zhu, R.K., Chen, Z.Q., et al., 2019. Organic-matter-rich shales of China. Earth Sci. Rev. 189, 51–78. https://doi.org/10.1016/j.earscirev.2018.12.002.